REINDEER

D2.3

Hardware requirements to support energy transfer to energy-neutral nodes

Project number:	101013425
Project acronym:	**REINDEER**
Project title:	REsilient INteractive applications through hyper Diversity in Energy Efficient RadioWeaves technology
Project Start Date:	1st January, 2021
Duration:	42 months
Programme:	H2020-ICT-52-2020
Deliverable Type:	Report
Reference Number:	ICT-52-2020 / D2.3 / 1.00
Workpackage:	WP 2
Due Date:	31st March, 2023
Actual Submission Date:	31st March, 2023
Responsible Organisation:	KU Leuven
Editor:	Jarne Van Mulders
Dissemination Level:	PU
Revision:	1.00
Abstract:	This deliverable reports on the evaluation and design of hardware resources needed for transfer of energy to energy-neutral nodes and backscattering-based connectivity to these nodes. The assessment of the hardware requirements takes energy efficiency as an important target, and includes different aspects such as synchronization, reciprocity calibration, and out-of-band constraints due to frontend non-linearities.
Keywords:	Wireless Power Transfer, Distributed large arrays, energy-neutral nodes

The REINDEER project has received funding from the European Union's Horizon 2020 research and innovation programme under grant agreement No 101013425.

Editor

Jarne Van Mulders (KU Leuven)

Contributors (ordered according to beneficiary numbers)

Chesney Buyle, Daan Delabie, Bert Cox, Jarne Van Mulders, Gilles Callebaut, Liesbet Van der Perre (KU Leuven)
Liang Liu, Ove Edfors (ULUND)
Benjamin Deutschmann, Thomas Wilding, Klaus Witrisal (TU GRAZ)
Ulrich Mühlmann (NXP)

Reviewers

Sai Subramanyam Thoota (LiU)
Pål Frenger (Ericsson)

Disclaimer

Executive Summary

This deliverable of the REINDEER project reports on the outcome of Task 2.4 and provides the required provisions at the infrastructure side for energy transfer to connect to and interact with energy-neutral nodes. The specific hardware requirements are assessed, taking into account the target to establish low complexity and energy efficient solutions.
The assessment presented in this deliverable mostly focuses on the practical deployment of wireless power transfer (WPT) from the distributed infrastructure to provide **good coverage** and potentially service **many devices**. Requirements assessed include the energy supply, antennas, power and hardware architecture and components. Specific limitations and implementation challenges are zoomed into. Backscattering approaches, proposing an elegant way to connect to energy neutral (EN) devices, are studied also in particular regarding transmission range and multi-device solutions when operating from distributed architectures.
The overall outcome of this deliverable is a comprehensive view on the **hardware requirements** at the infrastructure side to support energy transfer to energy-neutral nodes, in line with its major objective. Moreover, it discusses **algorithmic and procedural aspects** that have a major impact on these hardware requirements, e.g., regarding transmit waveform, synchronization, reciprocity calibration, and backscattering. A major conclusion is that even the most challenging use case considered in REINDEER can be served within the regulatory limits by the RadioWeaves infrastructure, which can benefit from **great transfer efficiency improvements thanks to the coherent operation from the distributed contact service points (CSPs)**.

Contents

List of Figures

List of Tables

Glossary

ADC analog-to-digital converter.

ASK amplitude shift keying.

AWGN additive white Gaussian noise.

BER bit error rate.

CDMA code division-multiple access.

CE channel estimation.

CSI channel state information.

CSP contact service point.

CW continuous wave.

DAC digital-to-analog converter.

DPD digital pre-distortion.

ECSP edge computing service point.

EDLC electrostatic double-layer capacitors.

EH energy harvesting.

EN energy neutral.

ESL electronic shelf label.

FA federation anchor.

FDMA frequency-division multiple access.

ICNIRP International Commission on Non-Ionizing Radiation Protection.

KPI key performance indicator.

LNA low noise amplifier.

LO local oscillator.

LoS line-of-sight.

LPF low-pass filter.

MC Monte Carlo.

MCU microcontroller.

MIMO multiple-input multiple-output.

MISO multiple-input single-output.

mMIMO massive MIMO.

MPPT maximum power point tracking.

MRT maximum ratio transmission.

NOMA nonorthogonal multiple access.

OFDM orthogonal frequency-division multiplexing.

OMA orthogonal multiple access.

OOK on-off keying.

PA power amplifier.

PAPR peak-to-average power ratio.

PE processing element.

PLL phase-locked loop.

PN pseudo-noise.

RCS radar cross section.

RE radio element.

RF radio frequency.

RFID radio frequency identification.

RIR reverse-link interrogation range.

RTF reader talks first.

RW RadioWeaves.

SA synchronization anchor.

SDMA spatial-division multiple access.

SISO single-input single-output.

SNIR signal-to-interference-plus-noise ratio.

SNR signal-to-noise ratio.

TCXO temperature compensated crystal oscillator.

TDD time division duplexing.

TDMA time division-multiple access.

TTF tag talks first.

VCO voltage-controlled oscillator.

VNA vector network analyzer.

WPT wireless power transfer.

Chapter 1

Introduction and system parameters

Connectivity to energy-neutral devices is a novel functionality targeted in 6G which is envisioned to enable new use cases in different environments, as introduced in deliverable D1.1 [1]. Indeed the possibility to interact with many things based on low cost labels that may not need a battery, opens opportunities to for example efficiently track and trace goods, support transformation of working and living environments, and develop novel games. This deliverable gives an overview of the functional and architectural requirements to support wireless power transfer in RadioWeaves enabled interaction with EN devices. It refines the general architectural concepts presented in REINDEER deliverable D2.1 [2] where RadioWeaves architectures are proposed to serve different wireless functions to support the requirements of novel use cases. The first WP2 deliverable also introduces adequate terminology for the novel distributed communication-computation infrastructure.

The CSP is introduced in D2.1 and consists of a Sensing Element (SE), a Processing Element (PE), a Charging Element (CE) and a Data Storage Element (DSE). The main focus here is on defining the optimal recommendations specifically for wireless power transfer, hence related to the CE, while disregarding communication requirements. Deliverable D2.1 has introduced wireless power transfer for RadioWeaves in section 6.3. The benefits of a distributed RadioWeaves architecture for WPT was demonstrated through preliminary simulations. The results have indicated that a high array gain is achievable, and that the multiple-input single-output (MISO) operation results in considerably lower path losses compared to single-input single-output (SISO) systems. The architecture to support coverage for EN devices was also already introduced in D2.1 (Section 6.3.4). Here, a more comprehensive analysis will be explored, discussed in Section 3.1.

We assume in the project and this deliverable that the energy to power the energy-neutral devices comes from CSP devices only. One or multiple radio elements (REs) from the CSP will ensure power delivery to the devices, operating in one or multiple frequency bands considered in REINDEER: $900\,\mathrm{MHz}$, $2.4\,\mathrm{GHz}$, $3.8\,\mathrm{GHz}$, and 5 to $6\,\mathrm{GHz}$. Other elements of the infrastructure can be responsible for the management of the WPT procedures and scheduling. These may include the **federation anchor (FA)**, when needed for the synchronization a **synchronization anchor (SA)**, resources to provide localization of nodes, etc., that may be required to realize the energy transfer.

This deliverable clearly is closely linked to WP4 focusing on interaction with EN devices and other WP2 deliverables detailing solutions for networking in distributed massive MIMO (mMIMO). In particular the following results presented in related REINDEER deliverables are of interest to

get a more comprehensive understanding on the methods and solutions to power EN devices in a RadioWeaves-based network:

- D4.1 introduces the main elements of an RF WPT architecture and discusses the hardware requirements at the EN device side. In contrast, this deliverable focuses on the CSP side. The benefits of multiband signals, which was already briefly discussed in D4.1, are explored more comprehensive. Further, ready-to-use RF harvester efficiencies are illustrated as reference case for the challenging electronic shelf label (ESL) use case, which is elaborated in this deliverable.
- D4.1 also provides a detailed discussion on the applicable regulations, as summarized and related to in this deliverable.
- The initial access for EN devices is covered in D4.2, where also signaling for energy harvester efficiency improvements is proposed.
- The closed loop approach to enable coherent operation in a distributed architecture and the possibility to use backscattering for the pilots to establish this approach are explained in detail in D4.2. This deliverable complementary handles the CSP hardware architecture enabling this closed loop approach in a distributed infrastructure.
- Synchronization for coherent operation in distributed wireless power transfer approaches is discussed in D2.2.

Major system parameters and symbols. This deliverable in line with the focus of the REINDEER project further assumes TDD operation and reciprocity-based beamforming.

This deliverable is further organized as follows. The next chapter first shortly revisits the use cases leveraging on EN nodes, and considers the overall wireless power transfer system in terms of energy and power requirements and efficient. Chapter 3 focuses on the options and techniques to provide and enhance coverage and service multiple devices. Next, limitations and implementation challenges are discussed in Chapter 4. The specific hardware requirements for the CSP are elaborated on in chapter 5. Chapter 6 zooms in on the backscattering technique to connect to EN nodes. Finally, the requirement are summarized and major conclusions are formulated in Chapter 7.

Chapter 2

Wireless power transfer to energy neutral devices

This chapter provides the top-down view on the requirements of the distributed RadioWeaves infrastructure to power EN nodes, starting from the needs of novel applications expected to be supported in 6G networks. This chapter leverages on the approaches introduced in D4.1 [3]. The relevant use cases are shortly revisited in the first section of this chapter, while the following respectively treat energy supply, antenna options, and input power requirements at the EN side. The latter is further considered in the remaining of this deliverable to determine the radiated power levels that should be generated by the infrastructure and the, potentially cooperating, CSPs in particular.

2.1 Use cases recap

Deliverable D1.1 [1] identified thirteen use cases within four main application domains where RW has the potential to bring considerable technological and societal advantages. These applications domains include (I) adaptive robotized factories, warehouses, retail and logistics, (II) immersive entertainment for crowds of people, (III) human-machine interaction in care environments, hospitals and assisted-living, and (IV) home automation and smart home systems. Detailed technical requirements and specific key performance indicators (KPIs) were defined for each use case, providing relevant and measurable values for evaluating the RW performance.

This deliverable investigates the hardware requirements of CSPs with WPT capabilities. To obtain realistic specifications for these hardware blocks, we rely on representative use cases that may benefit from this functionality. Some applications require substantial computational power and hence not all use cases stated in D1.1 [4] are relevant to this study. Table 2.1 gives an overview of use cases and their corresponding KPIs that are considered in drawing up the necessary WPT hardware requirements. By dividing the power density with the device density, we are able to calculate the DC power that needs to be delivered by the device's power circuitry in order to support the desired application.

Table 2.1: Key performance indicators related to wireless power transfer.

Application Domain	Application	Power density [mW/m^2]	Devices density [per m^2]	DC Power [mW]	Carrier frequency [GHz]
I	Electronic Labelling	0.24	20	0.012	2.4 5+
II & III	People Tracking	0.1	2	0.05	0.9 2.4 3.8 5+
III	Patient Monitoring	<1	2	<0.5	0.9 2.4 5+
III & IV	Smart Home Automation	0.25	100	0.0025	2.4 5+

2.2 Practical considerations in radio frequency wireless power transfer

Table 2.1 shows the DC power required by a device to fulfil its intended application. However, the RF power that ultimately needs to be available at the input antenna of the device should be considerably higher because of two main reasons: energy harvester efficiency and energy buffer leakage. This section will briefly discuss how and to what extent these parameters will affect the CSP hardware requirements.

2.2.1 RF energy harvesting efficiency

Deliverable 4.1 (System design study for energy-neutral devices interacting with the RadioWeaves infrastructure) [3] initially provided a model of a WPT link. The typical blocks involved in RF power transfer are again summarized in Figure 2.1. RF power is generated by one or multiple CSPs at the RW infrastructure. Affected by the wireless channel, the RF waves propagate to the receive antenna of a RW device, after which the rectifier performs the essential conversion from RF to DC power. This DC power can either be consumed immediately by the EN device (load) or stored in an energy buffer such as a supercapacitor.

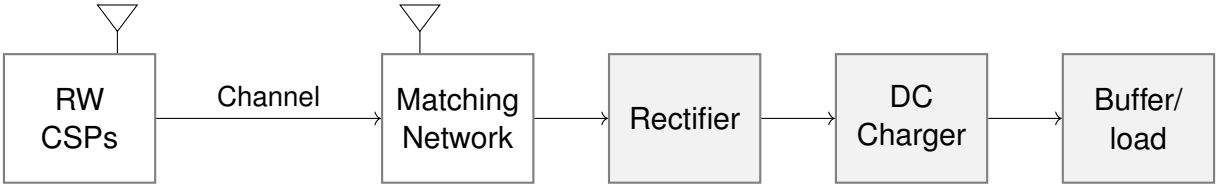

Figure 2.1: Radio frequency wireless power transfer link and receiver architecture

The entire conversion, however, does not come without losses in and between each of the blocks. The remainder of this paragraph focuses on the losses in the RF to DC power conversion, ultimately requiring a higher RF input power to meet the DC needs.

1. **Matching network**. When the output impedance of the receiver antenna does not match with the input impedance of the rectifier, power losses will occur due to reflections. Therefore, a matching network must be applied to tune both blocks to each other. Impedance matching in energy harvesting is, however, challenging because the impedance of the following rectifier circuit is highly dependent on the operating frequency, input power and load impedance [5]. Moreover, matching networks typically consist of passive components where parasitic components will cause additional energy losses. Ideally, the impedance of the antenna is matched directly to that of the rectifier, making the matching network obsolete and avoiding the associated losses. This conclusion was also drawn in evaluation of the power harvesting efficiency of D4.1 (Section 5.2) [3].

2. **RF to DC efficiency: rectifier**. The rectifier converts the high-frequency RF signal into DC power. This involves losses occurring in the diodes that make up the rectification circuit. The RF to DC efficiency can be improved through the choice of the rectification element as well as the rectifier topology. The rectifier design presented in D4.1 reported a harvesting efficiency of $40\,\%$ using an RF charge pump implementation. Looking at the commercially available AEM30940 RF energy harvester from E-peas [6], maximum efficiencies up to $60\,\%$ have been reported, even including the matching network efficiency.
3. **DC to DC efficiency: DC charger**. A DC-DC converter converts the output voltage of the rectifier circuit to the desired operating voltage. The rectifier's output voltage can also be tuned directly to the desired voltage level using for example a multiplier rectifier topology, making a DC-DC converter obsolete. In order to extract maximum power from the RF source, it is critical to operate at the optimum impedance. DC-DC converters with built-in maximum power point tracking (MPPT) functionality provide automatic impedance adjustments. This conversion can be combined with a Constant Current (CC) and Constant Voltage (CV) gradient to charge a certain type of energy buffer such as a capacitor, supercapacitor or battery.

Figure 2.2 shows the implementation block diagram of a typical EN device without external storage capabilities, and thus purely passive operation. Here, the antenna is directly matched to the input impedance of the IC and connected to RF1 and RF2 terminals. This avoids additional losses in the matching network and increases sensitivity. The analog front end (AFE) consists of a rectifier, a voltage regulator, modulator, demodulator, and adjustable antenna trimming capabilities. The digital control module integrates the required protocol handling (protocol state-machine and anti-collision handling), and data and memory management. Operational frequency is in the range from 868MHz to 2.4GHz, dependent on the antenna design. This EN device can operate approximately down to -23dBm available RF power below 1GHz. In this range, the RF-to-DC conversion efficiency is around 45%. Details on the performance are provided in D4.1.

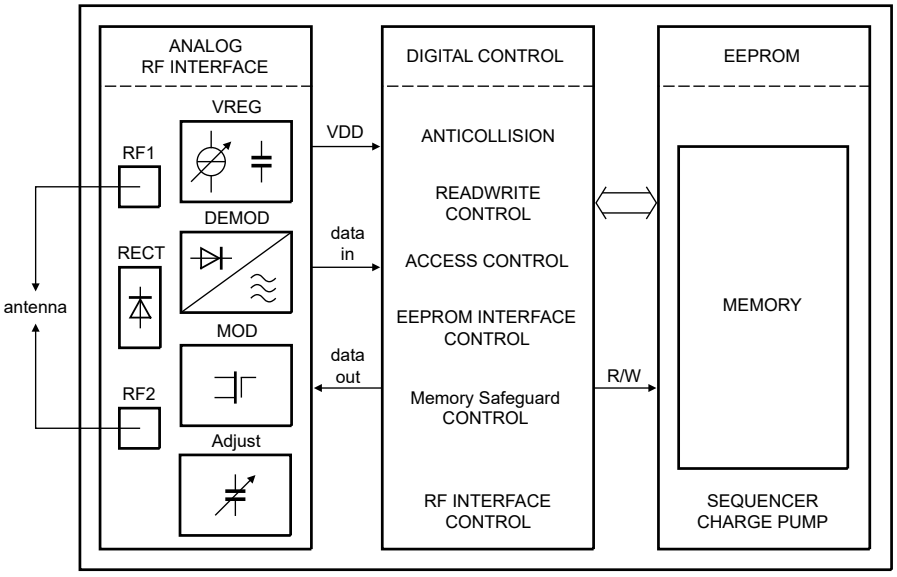

Figure 2.2: RF energy harvester IC implementation [7].

The AEM40940 integrated circuit is one of the few commercially available harvesters specifically for RF harvesting with matching circuit suggestions, built-in rectifier, and built-in voltage converter. Like its competitive counterparts, the DC-DC converter is equipped with MPPT functionality. The

datasheet represents the efficiency as a function of its input power for several frequency bands, as shown in Figure 2.3a: 867 MHz, 921 MHz and 2.4 GHz. These graphs clearly show the non-linear behavior of the energy harvester with an efficiency depending on the input power. Moreover, the reported numbers confirm and clarify that the losses in the harvester are considerable and should be taking into account when budgeting transmit power and energy at the infrastructure side. The efficiency data is converted to the DC output power related to input power and shown in Figure 2.3b [8].

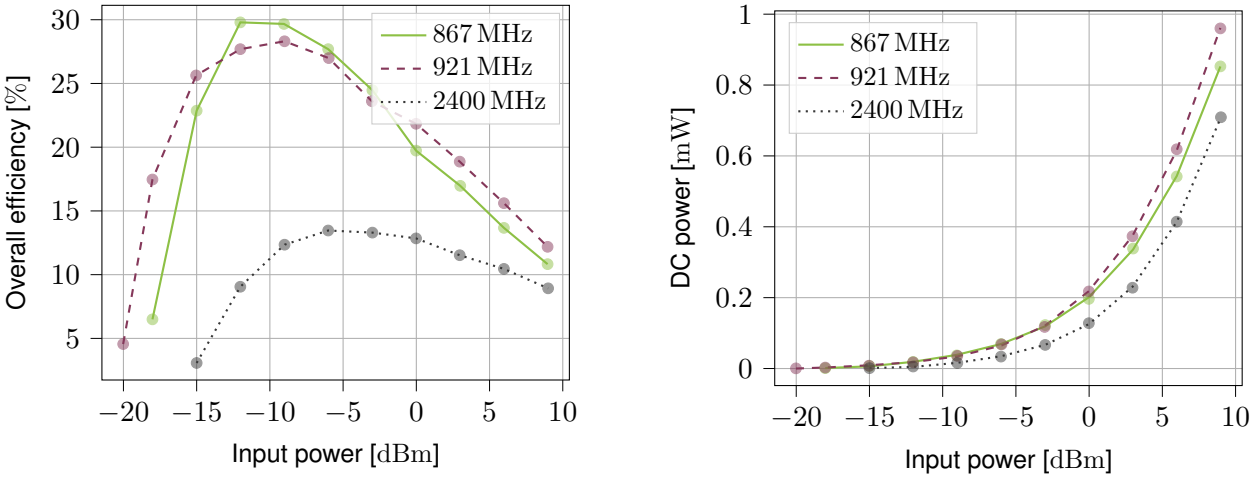

(a) Harvester efficiency

(b) DC output power vs input power

Figure 2.3: AEM40940 RF energy harvester [8].

2.2.2 Energy buffer leakage

In several use cases, the incident RF power is insufficient to power the EN device or perform its intended functionality right away. Consequently, RF power must be harvested over a longer period of time and the energy must be collected in some type of buffer. Taking the example of a supercapacitor, the dielectric insulator separating the conductor plates does not offer perfect insulation. A very low current will flow through the insulator, called the leakage current, causing the capacitor to discharge slowly over time. The typical leakage current of a capacitor is on the order of microamperes, and is affected by factors such as the dielectric material, ambient temperature and voltage rating [9].

Depending on a use case, trade-offs may arise in charging an EN device efficiently. Consider for example an use case where an EN device consumes a considerable amount of energy to execute a certain action, yet only a few times a day. On the one hand, one could allocate a large amount of resources to create a high power RF spot at the EN device for only a short time. However, due to the non-linear behavior of the energy harvester, the power conversion may happen at a lower efficiency compared to a lower RF input power. In this case, losses due to buffer leakage will be low as the collected energy can be consumed rather immediately. On the other hand, you could also allocate less RW resources that transmit a lower power spot continuously over a longer period of time. In this case, the energy harvester may operate at a higher efficiency, yet leakage losses can slowly add up. Hence, a lot of parameters such as availability, energy needs, energy harvester efficiency, and energy buffer leakage current will greatly affect the optimal charging strategy.

2.3 Required DC energy for a particular challenging use case

In this section, specific use cases described in D1.1 are considered in more detail. The goal is to define and estimate the required transmit power that should be radiated by the antennas. The latter will be discussed in Chapter 3. Different deployment scenarios such as tennis arena, production hall, supermarket, large apartment and patient care were introduced in D1.1. It would take us too far to comprehensively simulate and discuss all use cases. For simplicity, we further in this report consider the most challenging deployment scenario based on the assessment presented in Table 2.1, namely the supermarket equipped with ESLs is considered as a representative. These devices are assumed to be of EN class 1. Figure 10 from D1.1 describes the supermarket layout with a $5\,\mathrm{m}$ high ceiling and dimensions of $60\,\mathrm{m}$ by $30\,\mathrm{m}$. To reduce complexity, one aisle is considered with neighboring antenna arrays that can be enabled to feed the EN devices. Within an aisle, a federation with one FA is assumed to control the antenna resources in an optimal manner to provide sufficient RF power to all EN devices.

Figure 2.4 shows a 3D sketch of the considered shop aisle with dimensions $20\,\mathrm{m}$ by $4.4\,\mathrm{m}$ and $2.5\,\mathrm{m}$ high cabinets. The shelves of the cabinets have a width of $1\,\mathrm{m}$ and the cabinets have 6 shelves. Three antenna arrays, consisting of lambda/2 placed antennas, are located at $(0, n, 3)$, $(2.2, n, 5)$ and $(4.4, n, 3)$ [m]. With $n = \sum_{l=0}^{M} l \cdot \frac{\lambda}{2}$ and M the number of antennas in one antenna array given by $M = 20\,\mathrm{m} \cdot \left(\frac{\lambda}{2}\right)^{-1}$. Assuming a carrier frequency of $868\,\mathrm{MHz}$, 117 antennas in each array can be placed in the $20\,\mathrm{m}$-long aisle. In total, we consider 351 available antennas in this particular case for one aisle. The total number of transmit antennas is indicated as L ($= 3M$).

The use case analysis defined that there can be up to 600 ESLs in a shop aisle. The daily required DC energy is related to the ESL refresh rate and the energy to perform an ESL screen update. The largest consumer of one ESL device is the E-Ink Raw Display. In D1.1, it was stated that it takes $450\,\mathrm{mJ}$ ($15\,\mathrm{s}$ x $30\,\mathrm{mW}$) to update the display. Additional energy is needed to power the microcontroller (MCU) and demodulate the downlink information. In total, $500\,\mathrm{mJ}$ of energy is required for one ESL screen update. Assuming this happens twice a day, an amount of $1\,\mathrm{Ws/day/ESL}$ of energy should be delivered, which corresponds to a constant net power of $12\,\mu\mathrm{W}$. It may be noted that the EN device should have a storage capacity to store enough energy to support one ESL update. Suppose the harvester can boost the voltage with an MPPT boost converter to $5\,\mathrm{V}$, then the buffer capacitor will have to be larger than $40\,\mathrm{mF}$ to store the $0.5\,\mathrm{J}$ of energy. This capacity is not readily available in common aluminium electrolytic capacitors. Electrostatic double-layer capacitors (EDLC) can offer an alternative to buffer this amount of energy. For example, the FYL0H473ZF KEMET capacitor with a capacity of $47\,\mathrm{mF}$ could be selected. The voltage rating, of this specific capacitor, is $5.5\,\mathrm{V}$.

The amount of DC energy to refresh the ESL and track the customers is hence defined, while the required DC power is not yet quantified and is further analysed in Section 2.5.

2.4 Antenna selection to energize electronic shelf labels

The antenna selection strongly impacts the performance of a RadioWeaves system. The considered antenna types, orientation and also achievable gain are clarified in this section.

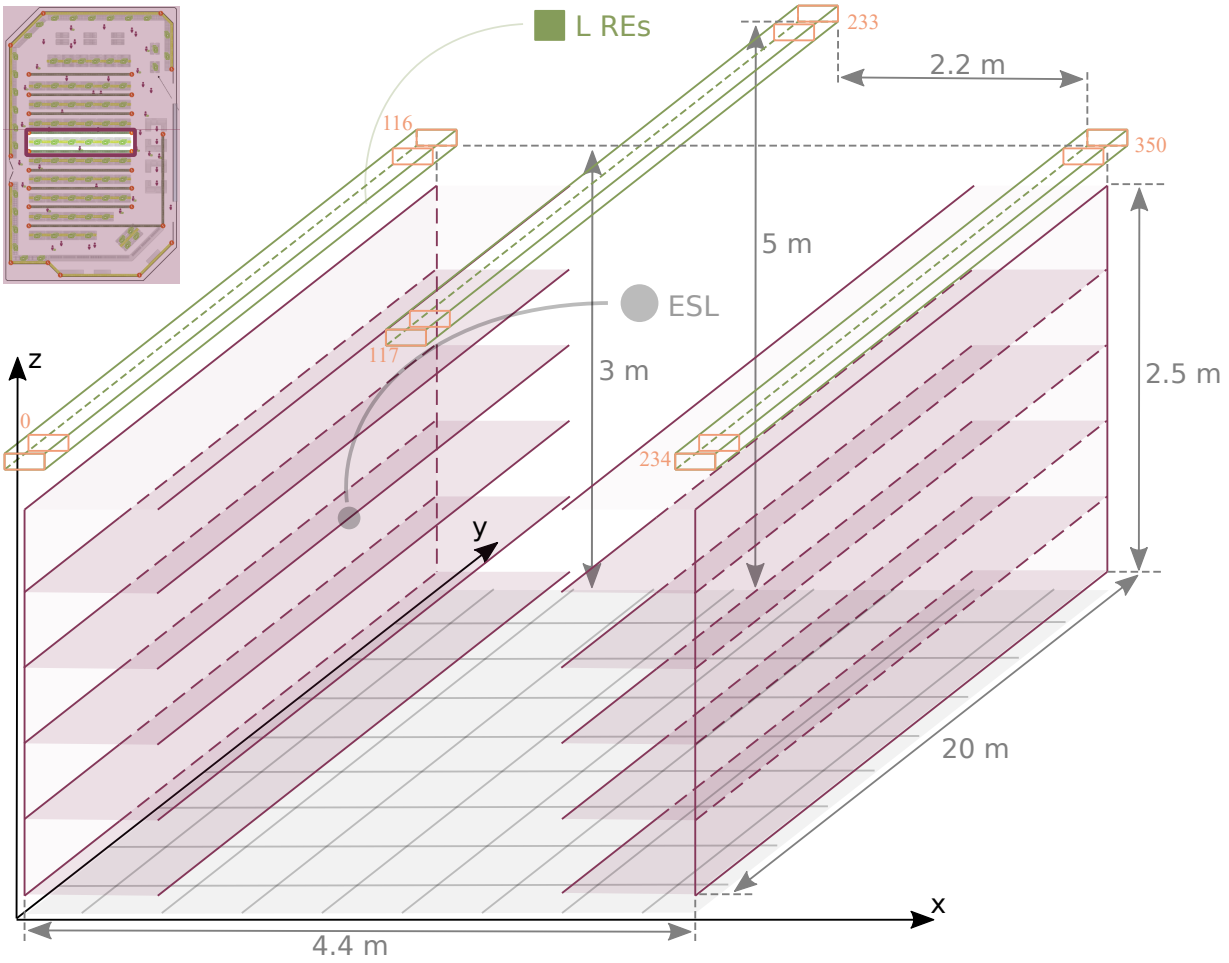

Figure 2.4: 3D representation of a supermarket aisle with 351 antennas transmitting on $868\,\mathrm{MHz}$. The orange digits represent the antenna numbering.

2.4.1 Antenna topology and orientation

Two antenna configurations are proposed that are considered in the calculations of the next section. Figure 2.5a shows the dipole configuration and Figure 2.5b visualizes the patch antenna orientation. Both the receive antenna (right figure) and one of the transmit antennas (left figure) are visualized in Figures 2.5a and 2.5b. To better represent reality, the patch antenna was assumed to be placed at an angle of $30°$, since this is usually the case for ESLs in supermarkets.

A half wave dipole antennas $(2.15\,\mathrm{dBi})$ with radiation pattern shown in Figure 2.6 and a patch microstrip inset-fed antenna [10] $(7\,\mathrm{dBi})$ with radiation pattern shown in Figure 2.7 are considered further in the calculations. The orientation of the dipole antennas is assumed to be parallel to the z-axis and the patch antennas in the arrays are placed parallel to the xy-plane. The polarisation losses will be neglected in this deliverable.

2.4.2 Antenna location and individual gain

Further estimates from Chapter 3 consider two representative ESL locations. The worst-located ESL is situated at a corner side with respect to the arrays with $(1, 0, 0)$ coordinates. The best-located ESL is found in a central location with coordinates $(1, 10, 2)$. Based on the transmit antenna locations and the ESL placements, the gain of the antenna can be determined. This

(a) Dipole antenna orientation

(b) Patch antenna orientation

Figure 2.5: Orientation of the transmit and receive antenna on the antenna arrays (infrastructure) side and the ESL side respectively.

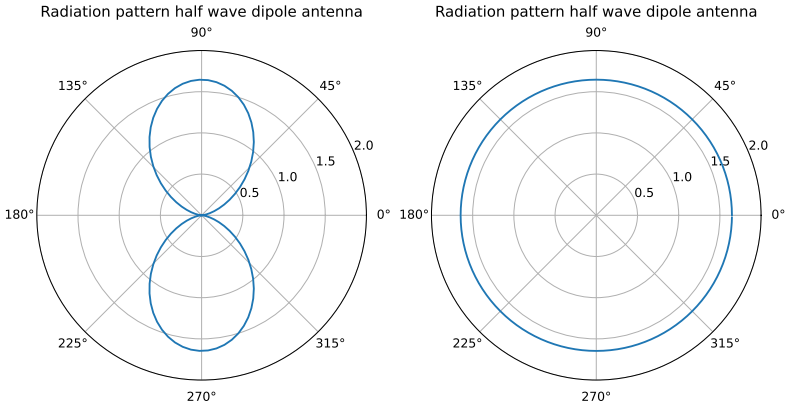

(a) Constant ϕ equals $0°$.

(b) Constant θ equals $90°$.

Figure 2.6: Dipole antenna with radiation pattern $G(\theta, \phi) = 1.646 \sin^2(\theta)$.

requires the antenna radiation pattern from Figures 2.6 and 2.7 in combination with the angle of incidence. The angle and thus the linear gain differs for each transmit antenna. The results for the closest located ESL and furthest located ESL are presented in Figure 2.8. The linear gain is calculated 351 times, i.e. for each situation. The three antenna arrays are visible in the figure through the abrupt change in gain from one antenna to another (visible at antenna number 116 to 117 and 233 to 234). The gain of the dipole antenna is the same for transmitter and receiver since these two antennas are parallel to each other (Figure 2.5a). Considering the situation with the patch antennas, the gain for transmitter and receiver differs from each other. The angle of $30°$ at the receiver increases the gain positively, especially for the transmit antennas from array 2 and 3 (antenna 217 to 350).

2.5 Required input RF power

2.5.1 Power requirements for positioning and/or tracking a device

D1.1 stated that passive tags can be engaged to track devices in factories, schools, hospitals, etc. Lets assume that people or devices are tracked in the aisle from Figure 2.4, then D1.1 estimated to facilitate thousands of passive tags, attached or integrated to the consumer goods in that space. The individual tag sensitivity is rated to be approximately $-23\,\mathrm{dBm}$. This provides sufficient power to the tag to communicate with the infrastructure. Passive tags use backscatter technology to communicate with the infrastructure, hence the position detection technology is mainly integrated in the infrastructure supported for instance with distributed antenna arrange-

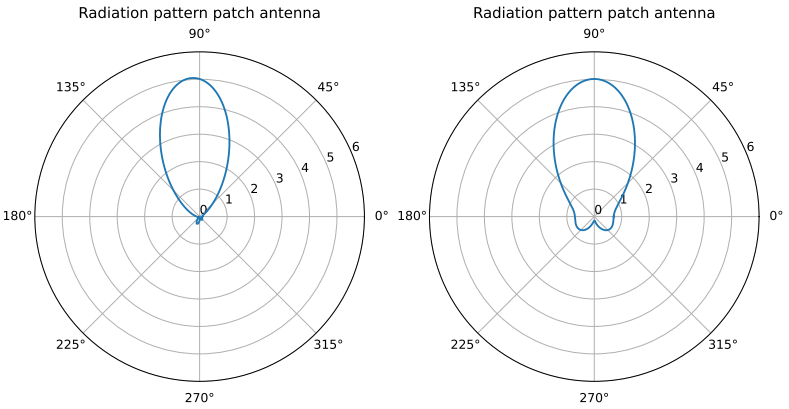

(a) Constant ϕ equals $90°$. **(b)** Constant θ equals $90°$.

Figure 2.7: Radiation pattern of patch antenna [10].

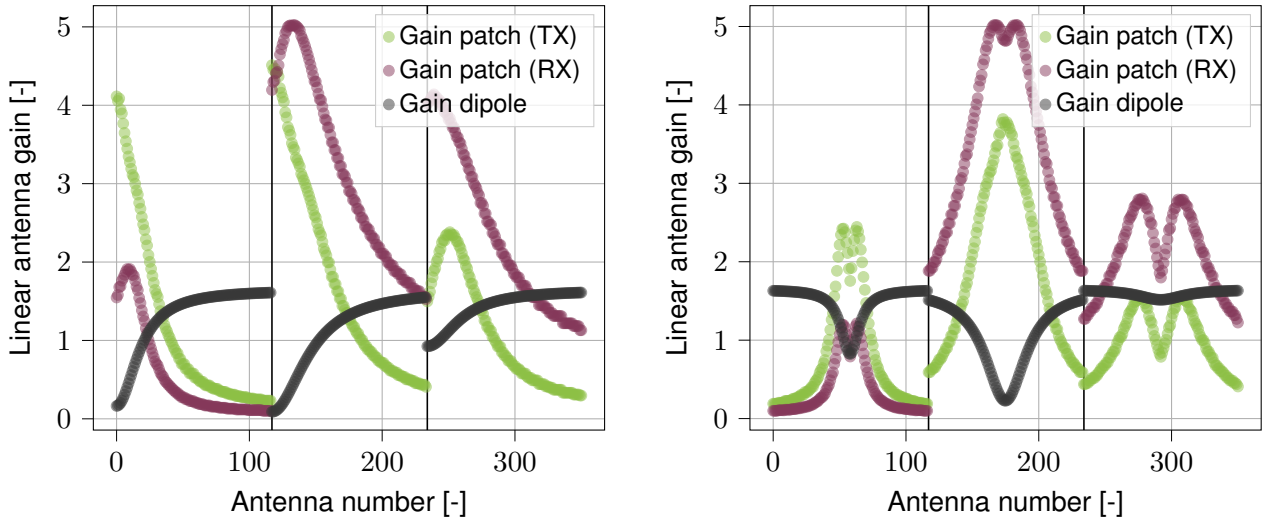

(a) Furthest located ESL **(b)** Closest located ESL

Figure 2.8: Linear antenna gain between ESL and each transmitter antenna

ments (multi-static). The tag supports the ranging signaling requirement in the backscatter modulation hardware to ensure ultra-low power operation. In case of an active ranging support feature, the tag sensitivity will decrease to a value in the range of $-10\,\mathrm{dBm}$ due to the required powering of an active transmitter. This means also that a storage device needs to be present, with an estimated capacity of $470\,\mu\mathrm{F}$ to survive short active communication bursts in the range of $100\,\mathrm{ms}$.

2.5.2 Power requirements for the ESL use case

Continuing the previous example from Section 2.3, no active communication is required and it is assumed that the location of the EN devices is determined during the installation process. Consequently, it is necessary to have a reference value regarding the minimum RF power to be received. Previous ESL requirements stated that a constant amount of $12\,\mu\mathrm{W}$ of DC net power is needed. This estimation assumed that the ESL can be powered and store energy nonstop continuously. To better assess the reality, the self-discharge of the energy buffer should also be included in the estimations, especially when the energy buffer is recharged over a very long period of time.

To determine the input RF power level, the harvester efficiency should be determined. Since there are many possible implementations of RF harvesters and the efficiency is not constant over the full input power range, the efficiency level is assumed to be constant for simplicity reasons. In the sequel, a harvester is assumed to have a constant efficiency of $30\,\%$.

Assuming that a constant net power of $12\,\mu\mathrm{W}$ should be received and taking into account losses in the harvester conversion, there should a receive level of at least $-14\,\mathrm{dBm}$ of input power. Note that this level is above the input sensitivity of most harvesters.

Chapter 3 will study whether, e.g., $-14\,\mathrm{dBm}$, power can be received at each ESL location. If this is not feasible, each device can be powered separately. Assuming 600 tags and 2 screen updates each day, there are $72\,\mathrm{s}$ of charge time to store $500\,\mathrm{mJ}$ of energy in the buffer. This equates to $7\,\mathrm{mW}$ of power to be received during each time period. Assuming that the harvester has an efficiency efficiency of $30\,\%$, the received RF power should be $23\,\mathrm{mW}$ or $\approx 14\,\mathrm{dBm}$.

Before going deeper into the calculations and estimation, the locations of the ESLs are illustrated in Figure 2.9. We assume in this deliverable that the 600 ESLs are divided over two YZ-planes (x = $1\,\mathrm{m}$ and x = $3.4\,\mathrm{m}$). The ESLs were numbered, also shown in the figure, which is crucial to understand the figures form Section 3.3.1. ESL-number 1 and 154 correspond with the furthest and closest located ESLs, respectively.

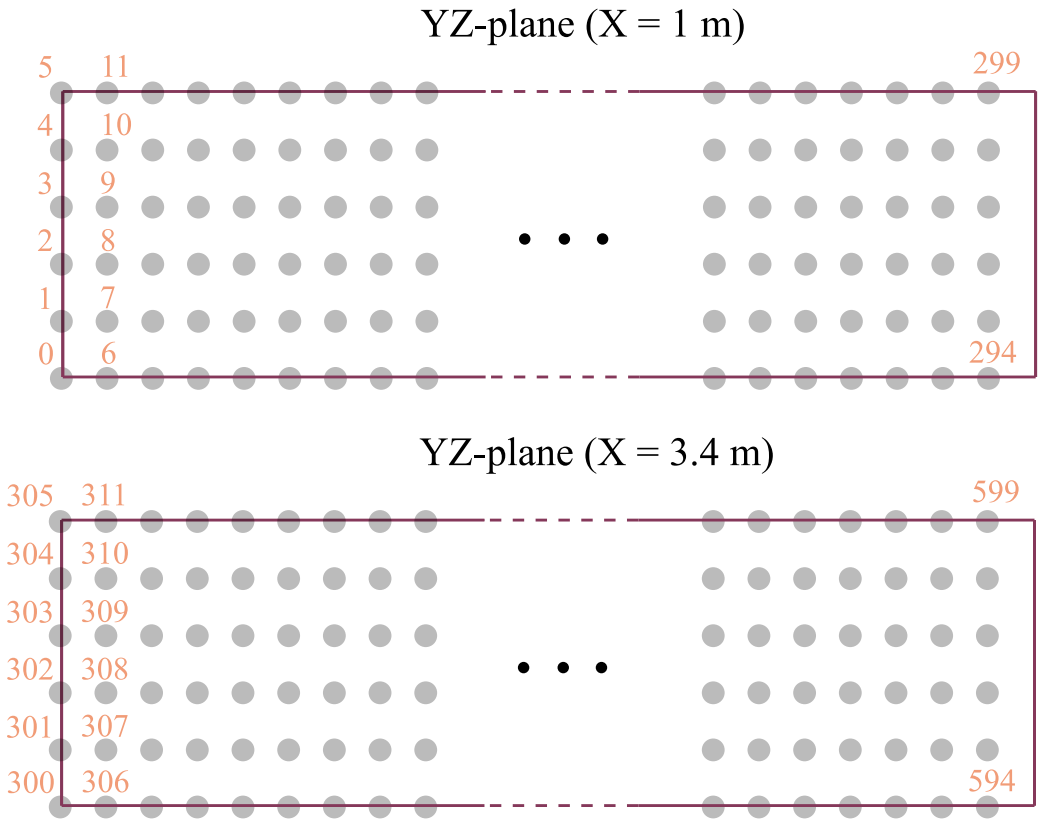

Figure 2.9: ESL indices and locations.

Chapter 3

Providing wireless power transfer coverage

This chapter describes coverage options to compare power transfer to EN devices along SISO on the one hand and MISO on the other hand, the latter operating either non-coherently or coherently. An estimation of the transmit power is provided using ideal calculations, supplemented by simulations with a better approximation of the real circumstances. This chapter further discusses techniques that can have an impact on the transmit power level. Beam sharing is considered and related to power spot size. The usefulness of multi-band operation and adequate transmit waveforms is also discussed.

3.1 Assessment of WPT coverage options

There are several implementation approaches to provide WPT to the EN devices. Section 6.3.3 from D2.1 *mapping to the architecture* already described two options concerning cooperative WPT from multiple RadioWeaves panels. A more extensive discussion is provided here.

Consider three CSPs installed against the walls with one EN device randomly placed in the environment, as proposed in Figure 3.1. The signals from each CSP can reach the EN device. The euclidean distances differ between the CSP and EN device d1 $<$ d2 $<$ d3. To provide sufficient energy on the desired location, four provisioning options are considered.

1. Option 1: One single antenna foresees coverage over the whole area. There are no other CSPs or they are not configured to act as a CE. For instance, they may miss the appropriate hardware and REs.
2. Option 2: Multiple distributed CSPs with corresponding REs can potentially provide energy towards the EN device. In this option it is assumed that only the closest CSP contributes to energy provisioning. A coarse-grained localisation system for estimating the best located CSP should reduce the charging distance of this SISO system and could improve efficiency compared to option 1. Moreover, other properties can be considered during the optimization, such as antenna gain. Despite the shortest distance of a given transmit antenna to the EN device, a slightly further situated antenna may provide better antenna gain and overall efficiency. In the example sketched in Figure 3.1, CSP 1 is the closest to the EN device and would be selected by the federation.

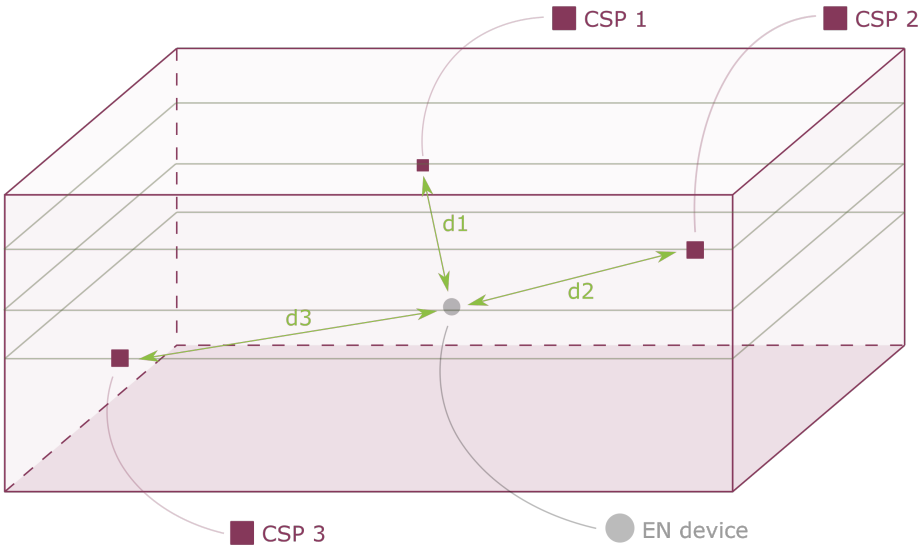

Figure 3.1: Providing energy to EN device with multiple CSPs. Each CSP contains one or more RE with potential beamforming properties.

3. Option 3: Non-coherent operation by multiple distributed CSPs. Multiple distributed CSPs with CE capabilities send out energy without synchronised radio elements. This non optimal way or RF energy delivery, yet unavoidable during the initial access procedure is explained in D4.2. From a hardware perspective, the complexity is low since specific synchronization elements and procedures could be neglected.
4. Option 4: Coherent operation by multiple distributed CSPs could generate a power spot at the EN devices location. The CSPs should be synchronized. This deliverable further discusses how coherent distributed beamforming can be supported at the hardware level.

These four briefly discussed coverage options are elaborated and further applied to the case study sketched in Figure 2.4 from Section 2.3.

3.1.1 Option 1 and 2: SISO operation antenna selection and efficiency

The infrastructure could power an EN device with one single RE. This means that if there are multiple EN devices, the same number of antennas will be active so that each device is assigned to one TX antenna. We assume the best placed antenna is selected to have the lowest path losses. At this point we neglect possible interference between the signals that could occur from multiple simultaneous SISO transmitters. This can be justified especially when there is a relatively high distance between multiple EN devices. Unlike Section 3.1.2, interference between multiple transmit signals is considered. In this analysis, it is assumed that there is a trade off between taking the closest transmit antenna or a better located TX antenna due to losses related to the antenna radiation patterns. Table 3.1 presents the distance d_{small}, referred to the closest located transmit antenna, as well as the most optimal distance $d_{optimal}$, related to the antenna with the lowest losses. The transmit power required to energize the ESLs, supplemented by the efficiency, is calculated in four situations. The quantity $PL_{optimal}$ represents the optimal path loss and $P_{tx,l}$ the transmit power with l the antenna number, retrievable in Figure 2.4.

No.	Location	Antenna	d_{small} [m]	$d_{optimal}$ [m]	$PL_{optimal}$ [dB]	l [–]	$P_{tx,l}$ [dBm]	Efficiency [%]
1	Shortest	dipole	1.4	1.7	-35.2	52	21.2	0.030
2	Furthest	dipole	3.2	5.2	-44.7	24	31.3	0.003
3	Shortest	patch	1.4	1.6	-27.6	54	13.6	0.17
4	Furthest	patch	3.2	3.2	-28.9	0	14.9	0.13

Table 3.1: Antenna selection, transmit power requirement, and overall efficiency for SISO operation. ESL requiring constant RF power of **-14 dBm** with 351 potential antenna locations of which the best-placed antenna is selected to power the EN device. The working frequency amounts $868\,\mathrm{MHz}$.

Table 3.1 reveals that transmit antennas with higher Euclidean distances with respect to the EN device, sometimes give better efficiency levels. Also, the transmit power can be reduced significantly by selecting a better situated antenna. The CSP hardware can in this case be simplified to an architecture without synchronisation requirements. A more comprehensive discussion on this architecture is provided in Section 5.1.1.

3.1.2 Option 3: Estimated CSP transmit power requirement for non-coherent MISO operation

Similar estimations are provided for the option combining the energy of multiple transmit antennas. A synchronized architecture is assumed to be unavailable, thus the transmitted RF power from the 351 antennas will interfere randomly. Equation (3.1) approximates the receive power for a non-coherent system $P_{rx,nc}$. Width L the number of antennas, $P_{tx,l}$ the transmit power per antenna l, and β_l the path loss between each transmit antenna and the EN device receive antenna.

$$P_{rx,nc} = \sum_{l=0}^{L} P_{tx,l}\beta_l \tag{3.1}$$

Equation (3.2) represents the simulated path loss model based on the Friis transmission equation. With $G_{tx,l}$ and G_{rx} the antenna gain and θ_l and ϕ_l the angles related to the incident RF beam that differs for each transmit antenna location. d_l represents the euclidean distance between the transmit antenna and the EN device.

$$\beta_l = G_{tx,l}(\theta_l, \phi_l) \cdot G_{rx}(\theta_l, \phi_l) \cdot \left(\frac{\lambda}{4\pi d_l}\right)^2 \tag{3.2}$$

Table 3.2 shows the results for the ESL use case presented in Figure 2.4. The calculations estimate the transmit power to achieve $-14\,\mathrm{dBm}$ of receive power, for the closest located ESL and furthest located ESL, and for both dipole and patch antenna configurations (Figure 2.8).

PG represents the path gain, $P_{rx,0dBm}$ gives the receive power if $P_{tx,l}$ equals $0\,\mathrm{dBm}$. To receive $-14\,\mathrm{dBm}$, the transmit power should be adjusted from $0\,\mathrm{dBm}$ to $P_{tx,l}$. Consequently, $P_{tx,total}$ represents $P_{tx,l} \cdot 10\log(L)$.

With 351 radiating antennas with random phases, the results show that at least $9.3\,\mathrm{dBm}$ of transmit power should be emitted in case of dipole antennas. For the implementation with patch

No.	ESL location	Antenna	$P_{rx,P_{tx,l}=0dBm}$ [dBm]	$P_{tx,l}$ [dBm]	$P_{tx,total}$ [dBm]	PG [dB]	Efficiency [%]
1	Shortest	dipole	-16.3	2.3	27.8	-41.8	0.007
2	Furthest	dipole	-23.3	9.3	34.8	-48.7	0.001
3	Shortest	patch	-11.9	-2.1	23.4	-37.4	0.018
4	Furthest	patch	-15.2	1.2	26.7	-40.6	0.009

Table 3.2: Transmit power requirement and overall efficiency for non-coherent MISO operation ESL requiring constant RF power of **-14 dBm**. All 351 transmit antennas could contribute to the total received RF energy. The operating frequency is taken to be $868\,\mathrm{MHz}$.

antennas, the transmit power can be further reduced to $1.2\,\mathrm{dBm}$. The proposed amount of transmit power is required to feed the ESL at the worst positioned location. Consequently, other ESLs with better and shorter locations, will receive more energy than actually needed.

Comparing Table 3.1 to Table 3.2, it appears that the efficiency is rather low, compared to a SISO system. Using multiple antennas to power an ESL results in lower efficiency levels. Note that the efficiency in this table is determined per ESL. Since there is no coherent operation by the infrastructure, the power will be averaged over the entire room. Assuming, 600 ESLs in the supermarket corridor, the approximate efficiency could increase by a factor of 600. Consequently, the overall efficiency level will end up higher compared to SISO operation, if multiple EN devices are considered.

3.1.3 Option 4: Estimated CSP transmit power for coherent MISO operation

The most efficient WPT option can be realised with coherent operation. However, this comes with extra complexity as it requires the infrastructure to synchronize CSPs in time, phase, and frequency to enable coherent operation. The discussion related to synchronisation challenges is further elaborated in Section 4.1. In order to achieve phase coherence, reciprocity calibration of the RF front-ends is needed. Aspects regarding the accurate calibration of the RF chains of the transceiver are discussed in Section 4.1.3. Further, Equation (3.3) represents the receive power estimation $P_{rx,c}$ with perfect constructive combination at the location of the EN device. Again, β_l can be substituted by Equation (3.2).

$$P_{rx,c} = \left(\sum_{l=0}^{L} \sqrt{P_{tx,l}\beta_l} \right)^2 \tag{3.3}$$

If we recalculate the receive power for the ESL use case we get the values for required transmit power and achieved efficiency presented in Table 3.3.

No.	ESL location	Antenna	$P_{rx,P_{tx,l}=0dBm}$ [dBm]	$P_{tx,l}$ [dBm]	$P_{tx,total}$ [dBm]	PG [dB]	Efficiency [%]
1	Shortest	dipole	11.1	2.9	28.4	-14.3	3.7
2	Furthest	dipole	3.9	10.1	35.6	-21.6	0.7
3	Shortest	patch	18.5	-4.5	21.0	-7.0	20.0
4	Furthest	patch	15.7	-1.7	23.8	-9.8	10.5

Table 3.3: ESL requiring constant RF power of **14 dBm**. All 351 transmit antennas could contribute to the total received RF energy. Considered working frequency is $868\,\mathrm{MHz}$.

The patch antenna achieves a high gain for the incident RF radiation perpendicular to the antenna surface. The gain related to the transmit antenna location was already demonstrated in Figure 2.8. As a result, an theoretical overall RF-to-RF efficiency can increase up to $20\,\%$[1] for the specific with the 351 coherently cooperating patch antennas, which is considerably higher than the dipole configuration. In addition, below $0\,\mathrm{dBm}$ of transmit power is required to recharge the ESL capacitor.

The total transmit power $P_{tx,total}$ falls within the limits of the regulations, as elaborated on in D4.1 [3]. The higher efficiency for the same amount of receive power evidently corresponds to lower transmit requirements. This is the case even assuming that the strength of power spots should be $14\,\mathrm{dBm}$ to generate the 1200 (600 ESLs x 2 updates per day) spots per day, which is $28\,\mathrm{dBm}$ higher compared to the non coherent case. It should be noted that these are still ideal approximations and simulations trying to mimic reality. Reflections and polarization losses were neglected.

3.2 Realistic assessment based on simulated channels

In the above assessment, some idealised conditions have been assumed, e.g., assuming line-of-sight (LoS) situations and no multi-path reflections. We have furthermore performed a more realistic analysis to estimate the transmit power requirements and achievable transfer efficiency performing simulations based on data from measurements of real channels. The channel model implemented in the simulator corresponds closely to the model described in Deliverable D2.1 [11]. Polarisation losses are not accounted for in the simulations, yet they could be easily added either by interpreting a specific deployment scenario or by simply assuming a $3\,\mathrm{dB}$ loss occurring when linearly polarized antenna(s) are used on one side of the link, and circularly polarized antenna(s) on the other side (as is commonly done in radio frequency identification (RFID)) [3]. This simulator-based assessment is performed specifically for the most efficient case of coherent MISO transmission, which we consider most relevant in the frame of a RadioWeaves infrastructure.

No.	Location	Antenna	$P_{rx,P_{tx,l}=0dBm}$ [dBm]	$P_{tx,l}$ [dBm]	$P_{tx,total}$ [dBm]	PG [dB]	Efficiency [%]
1	Shortest	dipole	8.9	5.1	30.6	-16.6	2.2
2	Furthest	dipole	3.7	10.3	35.8	-21.8	0.7
3	Shortest	patch	24.7	-10.7	14.8	-0.8	83.2
4	Furthest	patch	21.1	-7.1	18.4	-4.4	36.3

Table 3.4: Estimated transmit power requirements and transmit efficiency from simulations based on actual measured channel data.

The results of this assessment based on simulated channels are shown in Table 3.4. These demonstrated that again, significantly higher path gains are achievable compared to non-coherent operation. Compared to estimations by applying Equation (3.3) represented in Table 3.3, there is a huge increase in efficiency with patch antenna transmitters and receivers. It should be noted that the simulations take into account the shelves which serve as additional reflection surfaces. Previous ideal calculations neglected these surfaces. The higher path gains can possibly be explained by a favorable situation due to these additional reflections.

[1] Note that this is an impressive number for RF-based WPT over distances in the order of meters, this high number being achieved thanks to the optimal MISO operation in combination with the beneficial antenna orientations

3.3 Techniques to support multi-device operation and enhance coverage and efficiency.

We here discuss the opportunities offered by an infrastructure with distributed CSPs and supporting multi-band operation to improve coverage and connectivity to multiple devices in the environment. From the use cases analysis [1], it is clear that the latter is key as a massive number of EN devices may need to be serviced in one environment. Furthermore, the impact of the transmit waveform on the energy harvesting performance is discussed.

3.3.1 Beamsharing

The concept of *beamsharing* can be applied to wirelessly charge multiple ESL at the same time. This yields the possibility to reduce the overall transmit power or the transmission time, and avoid using antennas that contribute only marginally. Beamsharing can be implemented following two strategies: i) through sharing uplink pilots [12] or ii) via exploiting channel correlation between different ESLs. The former gives several ESLs the same uplink pilot. In the (uplink) channel estimation phase, the CSPs will estimate the joint channel responses of all the ESLs sharing the same pilot. When maximum ratio transmission (MRT) is used during WPT, the beam will be shared between these ESLs. As the joint channel is estimated and MRT transmission is performed, ESLs with a higher gain will receive more power. Hence, this method is inherently unfair. Another approach is to use the full channel state information (CSI) knowledge to group ESLs with correlated channels. Due to the high number of densely distributed ESLs, the probability that some ESLs share channel characteristics can be exploited. The high density supplemented with the indices was already illustrated in Figure 2.9. The spacing between the ESLs is $50\,\mathrm{mm}$ and $40\,\mathrm{mm}$ along the Z- and Y-axis respectively.

3.3.1.1 Power Spot size

The supermarket example illustrated in Figure 2.4 is considered. In the remainder of this section, we investigate the possibility to do beamsharing when we have 600 ESLs uniformly spread over the 6 shelves of each of the two racks. As a first exploration of beamsharing, we assess the power spot size when wirelessly charging one ESL at a time, assuming free space conditions (Equation (3.2)). The received signal strength and power spot size when targeting the furthest located ESL and closest located ESL are depicted in Figures 3.2 and 3.3 when using MRT with dipole antennas for a 2D plane of the environment perpendicular to the store cabinets with ($x = 1$). A $-3\,\mathrm{dB}$ threshold is used to delineate the power spot area (with respect to the received power at the target ESL). The spot area increases from $0.0457\,\mathrm{m}^2$ to $0.3967\,\mathrm{m}^2$ when moving from the best to the worst case position. Consequently, assuming a density of 20 devices per square meter, the probability that one of the remaining 19 EN devices (per square meter) is lying in this spot is $4.5\,\%$ for the best case location and $39.7\,\%$ for the worst case location.

We can conclude that for a situation with a few hundreds of devices in the environment, one may always expect some of them to automatically benefit from beamsharing. In case these sharing situations are somehow identified and located, this could be exploited in an optimized charging scheduling and hence improve overall efficiency. The latter can be in particular relevant for nodes in bad locations where efficiency is lower on the one hand, and beamspots and the possibility that they can be shared are larger on the other hand.

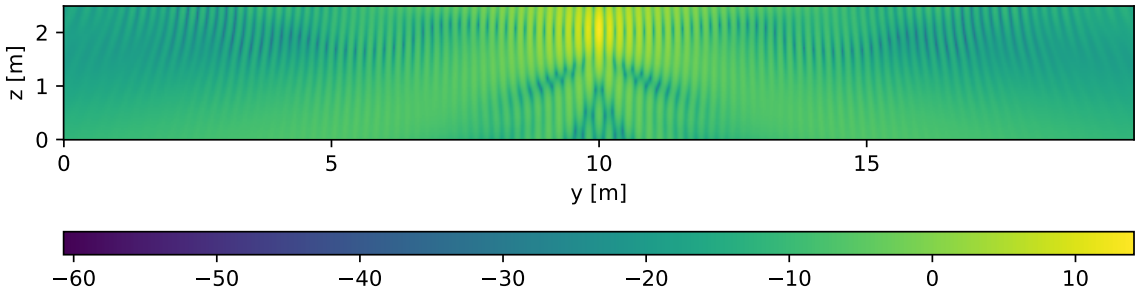

(a) Signal strength [dBm].

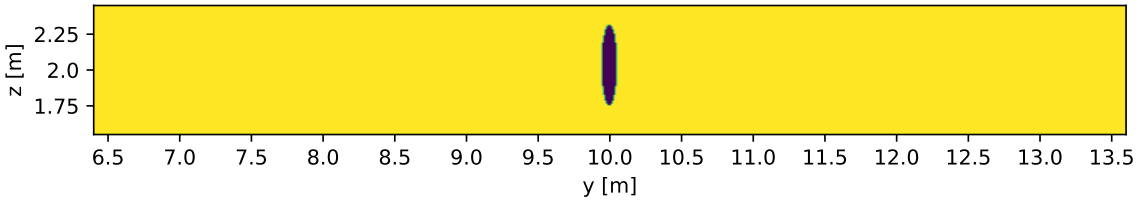

(b) Power spot size with a surface of $0.0457\,\mathrm{m}^2$.

Figure 3.2: Assessment for the power beamed towards the node at position No.1 (best case) from Table 3.3. (a) indicates the signal strength and (b) the power spot size in a 2D plane that is situated perpendicular to the shelves at $x = 1$ in Figure 2.4.

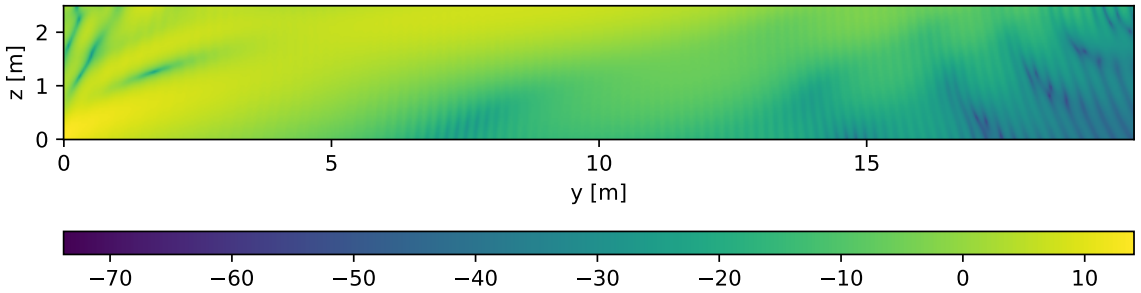

(a) Signal strength [dBm].

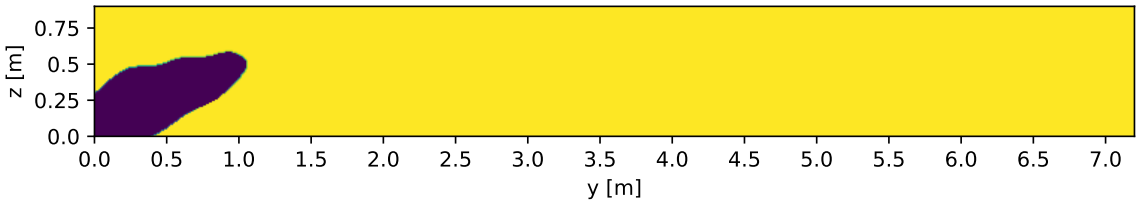

(b) Power spot size with a surface of $0.3967\,\mathrm{m}^2$.

Figure 3.3: Assessment for the power beamed towards the node at position No.2 (worst case) from Table 3.3. (a) indicates the signal strength and (b) the power spot size in a 2D plane that is situated perpendicular to the shelves at $x = 1$ in Figure 2.4.

3.3.1.2 CSI-based beamsharing

When the CSI is known for all the ESLs, this information can be used to group ESLs with correlated channels for WPT purposes. Figure 3.4 depicts the channel correlation matrix $\mathbf{R} = \mathbf{H}\mathbf{H}^H$, where $\mathbf{H} \in \mathbb{C}^{K \times M}$ contains the channel coefficients between each ESL k and antenna element m. The correlation matrix R illustrates the correlation between the channels towards the ESLs.

As illustrated in Figure 3.4, some ESLs show higher channel correlation with each other than others, which can be exploited during the wireless charging phase.

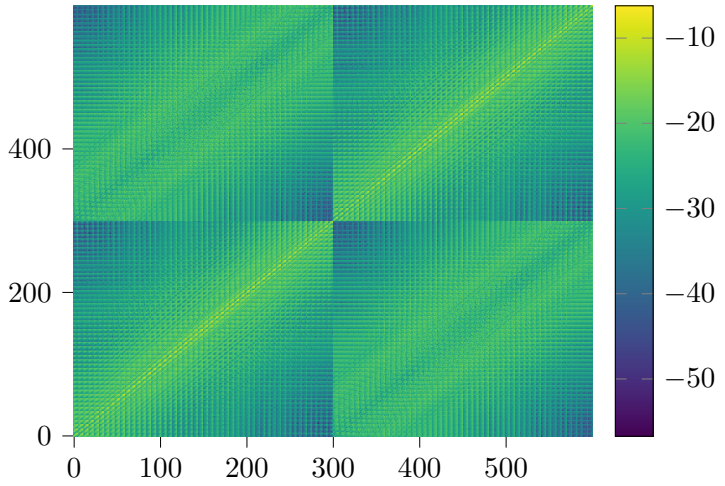

Figure 3.4: Channel correlation matrix $\mathbf{R}$. It illustrates which antennas are highly correlated with each other for the K ESLs.

To see the contribution of each antenna element to the channel correlation, all ESLs with a channel correlation above $-3\,\mathrm{dB}$ are selected for a given reference ESLs, i.e., taking a column of Figure 3.4 for a given target ESLs. Let P be the channel matrix of these grouped ESLs. The antenna correlation matrix $\mathbf{R}_{\text{ant}} = \mathbf{P}^H\mathbf{P}$, where $\mathbf{P} \in \mathbb{C}^{K_s \times M}$ and K_s is the number of *selected* correlated ESLs. This information can be used in the federation orchestration phase of the RadioWeaves network. Two examples are shown in Figure 3.5a and Figure 3.5b for the closest located ESL and furthest located ESL respectively. It shows that some antennas have a high correlation between the selected users, indicating that these antennas contribute more to the beamsharing than the others. In the federations stage, both $\mathbf{R}$ and $\mathbf{R}_{\text{ant}}$ can be used as performance metrics to i) group ESLs ($\mathbf{R}$) and ii) reduce the operational number of antennas ($\mathbf{R}_{\text{ant}}$) contributing significantly to the WPT.

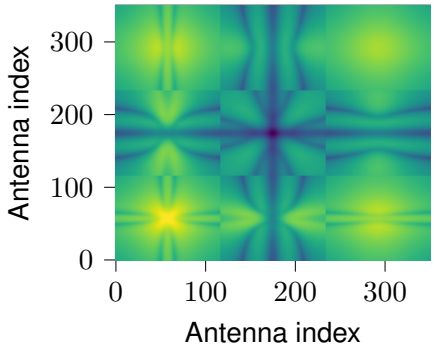

(a) $\mathbf{R}_{\text{ant}}$ of closest located ESL. The group size is 2 with ESL indices 154 and 155.

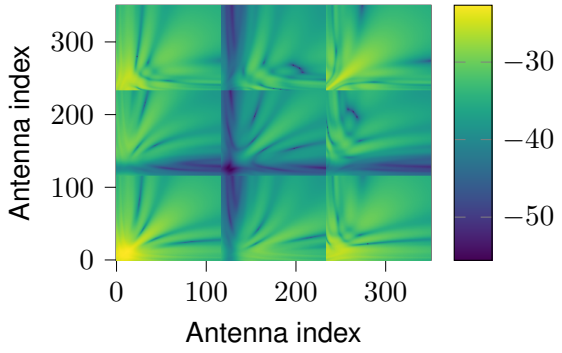

(b) $\mathbf{R}_{\text{ant}}$ of furthest located ESL. The group size is 8 with ESL indices 0, 6, 7, 13, 19, 21, 25 and 29.

Figure 3.5: The antenna correlation matrix $\mathbf{R}_{\text{ant}}$ of the grouped ESLs.

3.3.2 Multi-band operation

Multi-band operation for RF WPT exploits multiple frequency bands to increase the total amount of receive power and thus harvested energy. As stated in D4.1 [3], this could be interesting for

medium to higher power demanding applications, and to achieve higher localization accuracy or multi-band communication. The total harvested DC power ($P_{rx,mb}$) of a multi-band harvester with N contributing bands is given by:

$$P_{rx,mb} = \eta_c \sum_{i}^{N} G_i P_{RF}^{i} \, \eta_{RF,DC} \tag{3.4}$$

The RF to DC power conversion efficiency ($\eta_{RF,DC}$) contains the matching network efficiency, the rectifier efficiency and the DC charger efficiency, as discussed in Section 2.2.1, which here needs to be determined for every individual single-band link. G_i denotes the antenna's gain at the i-th frequency and η_c the DC combining circuit efficiency [13]. The harvested DC power can therefore be increased if an efficient DC combining circuit is used. Combining DC voltages typically can be achieved with two approaches: voltages are either combined after the rectifiers or after the DC/DC converters to charge a common storage element. A matching circuit and rectifier need to be provided for each band to maximize the overall efficiency, yet this negatively affects the overall complexity, cost, weight and size of the EN device [14]. Different types of rectifiers are used in practice. A distinction can be made between the series, parallel, and Greinacher rectifier, with the latter being by far the most commonly used due to the higher DC output voltage levels [13], [15]. The number of stages within this voltage multiplier affects the RF to DC efficiency, voltage output, and design of the matching circuit, and this moreover depends on the exploited frequency band. More specifically, increasing the frequency or number of stages decreases the impedance of the voltage multiplier [14], [16].

In general, the efficiency of a multi-band WPT system is reported to be higher than that of a single-band system [14]–[17] since additional energy is transferred from the antenna to the rectifiers of the other bands, even when the non-ideal impedance matching is taken into account [16]. The efficiency strongly depends on the input power [13], load [15], and frequency band [14]. Higher frequency bands cause lower efficiency compared to lower frequency bands at the same RF power density, due to parasitic element losses. Besides, more coverage is possible at lower frequencies due to the smaller path loss. The duty cycle regulations and energy harvester ICs are typically more optimal for lower frequency bands [18].

Due to the increased design complexity of the EN device, since multiple impedance matching networks, specifically designed antenna's, multiple rectifiers and DC/DC converters are needed, we opt to not further consider multi-band devices within REINDEER. The single-band operation makes it possible to design a simpler, less expensive, smaller and lighter EN device. The fact that this goes along with a reduced performance is less problematic since the target use cases, as mentioned in Table 2.1, have a relatively low power specification and a low update rate. Besides, the multi-band operation can only increase the total amount of energy transferred but does not offer a growth in coverage, with the latter being the main limitation to encounter. If an EN device still needs to use multi-band WPT, for example to improve positioning accuracy or communication throughput, and this device has the necessary hardware, the REINDEER concept can easily be extended to a multi-band system since multi-band antennas have already been designed for the CSPs. However, the operation of the WPT concept can be demonstrated via single-band operation.

3.3.3 Transmit waveforms

This section briefly discusses the dedicated transmit waveforms that could be generated by the CSP radios to increase WPT performance or to have downlink communication. This information can be further related to the hardware requirements in Chapter 5. Specific and comprehensive waveform design related to communication is not discussed in this deliverable.

3.3.3.1 Increasing harvesting performance by multi-tone excitation

Previous research has studied the impact on rectifier circuits for several types of input waveforms to increase efficiency. Beside a single tone continuous wave (CW) signal, other signals such as two-tone CW signals, chaotic waveforms, pulse signals, analog and digital modulated signals, frequency-shift keying signals, white noise, and orthogonal frequency-division multiplexing (OFDM) signals have been proposed [19]. In general, higher peaks yield higher efficiency levels because of the non-linear behaviour of the diode. The harvester efficiency depends both on the carrier frequency and the input power level. The frequency dependency is due do the matching network characteristics, while the input power dependency is explained by the non-linearity of the diode model. This field of research is treated in REINDEER deliverable D4.2 [20], where it is explained that not every rectifier circuit is suitable to achieve efficiency gains with high peak-to-average power ratio (PAPR) signals.

From a CSP perspective, it is primarily interesting to generate high PAPR signals, only if analysis results show a potential to achieve RF to DC efficiency gains at the EN device harvester. Since gains are not per definition achievable [19], it is highly recommended to firstly simulate the signals under the expected circumstances. [21] shows, e.g., the impact for a range of loads on the efficiency. This research shows efficiency gains with multi-sine signals for a restricted ranges of loads and even efficiency drops for low resistant loads. In short, sufficient research on the circuit design is crucial to avoid even poor efficiency compared to single tone signals. Most research such as [19], [21] focuses on RF to DC conversion via a single diode. These RF to DC circuits have proven to achieve higher conversion gains on peak signals with respect to constant-envelope signals. If the received power increases due to increasing efficiency, in fact the coverage area also expands. Still, the system will not reap benefits from an overly complex implementation. Chapter 3 showed that the single tone approach could deliver enough energy to the EN devices without exceeding the regulations for the ESL use case.

Generating multi-sine RadioWeaves signals is more challenging to support. The infrastructure should have control over the start of the multi-sine signal envelope period, beside the phase of the carrier frequency. Among phase synchronisation, also time synchronisation is required to provide overlap of the varying envelope signals (coming from different transmitting locations) at the desired (EN device) location. Research on multi-sine RF-based WPT has shown that the additional complexity involved in realizing efficient transfer, in particular to achieve coherent transmission from multiple antennas, is significant [22]–[24].

Waveforms with a non-constant envelope impact the hardware, more specifically the selection and type of the power amplifier (PA). The related challenges and associated hardware to support the transmission of high PAPR signals is briefly discussed in Section 5.2.2.

3.3.3.2 Simultaneous power and data

Class 1 EN devices (as defined in the use cases catalogue in D1.1 **)** require simultaneous power and data transfer. This means that the power carrier needs to be always on during communication in both directions, uplink and downlink, because typically only a very small capacitor is integrated in the device to survive the modulation gaps only. However, before any downlink communication can be initiated, the power carrier should be on for a sufficient time to allow the device to stabilize the internal voltage references. After this initialization phase, the communication can start. To keep the complexity of the EN device demodulator very low, modulation signaling as illustrated in Figure 3.6 shall be considered.

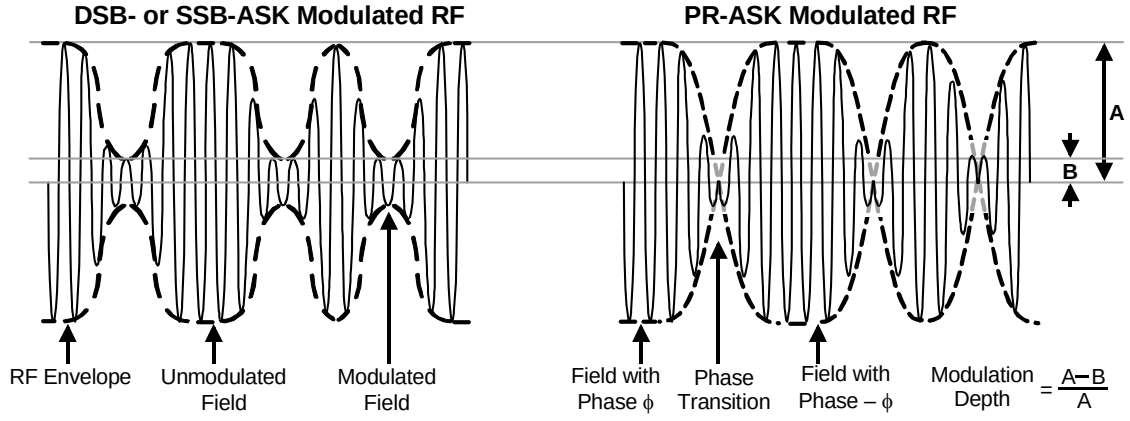

Figure 3.6: Proposed downlink modulation schemes: DSB, SSB, or PR-ASK modulation providing high modulation depth, copy of Figure H.1 in Annex H, pp. 143 of [25].

Specifically, the power carrier shall be modulated with double (DSB) or single-sided (SSB) sideband ASK, or phase reversal (PR) ASK. The modulation depth shall not be below 80%. Uplink communication should be backscatter modulation in this case, because this can be implemented with low complexity on the EN device modulator. Only a switching transistor across the antenna terminals needs to be managed with an on-off keying (OOK) digital signal train. In addition, this is also the simplest implementation of a simultaneous power and data transmission uplink. Overall, the modulation sequence shall be similar to the RFID Gen2v2 Specification, which is illustrated in Figure 3.7.

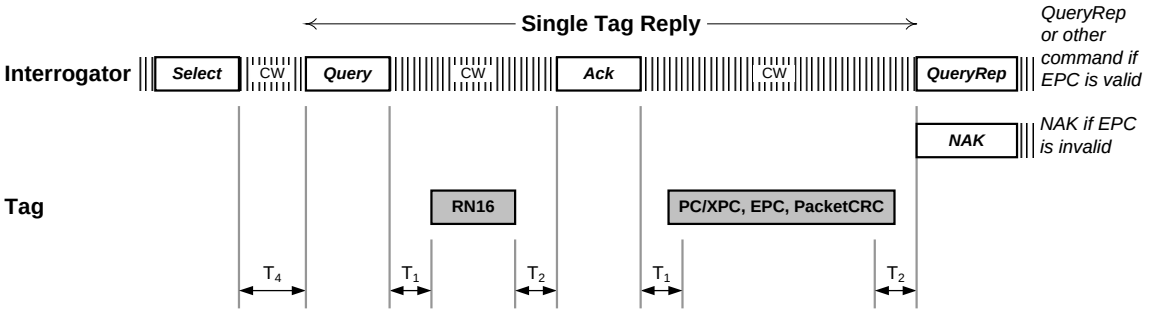

Figure 3.7: Protocol sequence of continuous power and data transfer, copy of Figure 6.18, pp. 42 of [25].

Here the interrogator is functioning as power carrier provider and communication initiator, whereby Select, Query, Ack, QueryRep, and NAK are specific downlink communication sequences, using modulation patterns as illustrated in Figure 3.6. The Tag, or EN device, responses with RN16 and EPC packet (e.g. electronic product code of a shelf item). The RadioWeaves infrastructure needs

to support this kind of simultaneous power and data transfer scheme to support electronic labels (RFID tags). Other use cases using custom specific class 1 EN devices might differ in terms of the protocol sequence given in Figure 3.7, yet they would have to follow downlink modulation schemes according to Figure 3.6 and device backscatter modulation to guarantee simultaneous power and data that allows low complexity hardware at the EN device.

Chapter 4

Implementation challenges and regulatory limitations

This chapter zooms in on specific implementation challenges to achieve coherent WPT operation, which has been shown to enable a significantly higher efficiency than SISO or non-coherent MISO operation, yet requires synchronization in time, phase, and frequency. Further, limitations due to regulatory constraints are discussed.

4.1 Coherent operation

There is a need for some cooperation between the different CSPs to achieve some levels of synchronization. The focus here is on the wireless power transfer requirements, supplemented with calibration options of the CSP hardware. The latter also has its impact on the support to transmit the desired signals and create a collaborative RadioWeaves infrastructure.

4.1.1 Architectures for coherent operation

A distinction can be made between time synchronization, frequency synchronization, and phase synchronization. We refer the reader to D2.2 [26] to consult the different implementation options to realize synchronization. Ideally, when there is a perfect synchronization between the CSPs, both drifts and offsets do not occur. If certain offsets are still present, they can be eliminated via reciprocity calibration from Section 4.1.3. Moreover, synchronization errors can be tolerated to some extent, as elaborated in Section 4.1.2.

Assuming perfectly synchronized RF front-ends and time-synchronized control logic, the infrastructure will be able to generate a beam spot by distributed beam-forming. In this case, the location of the EN device is considered to be known and the weight vectors are calculated via MRT. This working principle could be used in the ESL use case, where the position of the ESL is fixed and does not change over time.

Because of the limitations of previous methods and the unknown location in many use cases, it may be better to use the closed-loop approach explained in D4.2 [20]. In short, the proposed process consists of three steps. First, a non-coherent waveform is emitted by several REs. The buffer of the EN device can sufficiently charge. Secondly, a pilot is backscattered by the EN device, which provides each CSP with information about the location of and channel to this device.

Lastly, a re-transmission with the same phase relative to the internal CSP reference clock is sufficient to generate a power spot around the EN device. The architecture related to this approach is discussed in Section 5.1.2.

4.1.2 Consequences of inaccuracies in synchronisation

mMIMO systems can benefit from large array gains $G_{\text{array}} = L$ (where L denotes the number of transmit antennas in a MISO system) given fully phase-coherent operation and perfect CSI. In a realistic implementation, however, phase synchronization can only be realized with limited accuracy. Phase errors manifest in power losses which impact the system performance both for communication purposes due to a decreased signal-to-noise ratio (SNR), and for WPT due to lower power budgets.

4.1.2.1 Fundamental performance limits

In the following, we derive the fundamental performance limits of mMIMO systems subject to phase synchronization errors. We consider a MISO system with L transmit antennas transmitting power wirelessly to a single EN device. For channel state estimation and communication with the EN device, we consider time division duplexing (TDD) and reciprocity-based MRT. In [27], we derived the system efficiency, i.e., its path gain PG, for noisy channel estimates $\hat{\boldsymbol{h}} = \boldsymbol{h} + \boldsymbol{n}_h$ with the i.i.d. noise samples $[\boldsymbol{n}_h]_\ell \sim \mathcal{CN}(0, \sigma_h^2)$.
In this section, we derive the system efficiency with inaccurate phase synchronization. We model the received signal as

$$y = \boldsymbol{h}^{\mathsf{T}} \boldsymbol{s} + n \qquad \text{with } \boldsymbol{s} = \sqrt{P_{\text{tx}}}\, \boldsymbol{w} \tag{4.1}$$

where $n \sim \mathcal{CN}(0, \sigma_n^2)$ denotes complex additive white Gaussian noise (AWGN) and $\boldsymbol{s}$ is a transmit signal vector with a transmit power P_{tx}. The weight vector elements

$$[\boldsymbol{w}]_\ell = \frac{[\boldsymbol{h}]_\ell^*}{\|\boldsymbol{h}\|} e^{j\,\varphi_\ell} \tag{4.2}$$

are formed through MRT on the true channel $\boldsymbol{h}$ but each antenna $\ell \in \{1 \ \dots \ L\}$ suffers from i.i.d. synchronization errors $\varphi_\ell \sim \mathcal{N}(0, \sigma_\varphi^2)$. We further assume that the distributions of n and φ_ℓ are independent, and we assume that the power of the noise n (i.e., for ambient energy harvesting) is negligible when compared to intentional WPT.

We denote the channel power gain (which is actually an efficiency) by the average path gain of all L antennas, i.e., by $G_{\text{ch}} = \frac{1}{L}\|\boldsymbol{h}\|^2 \approx PG_{\text{SISO}}$. Through the definitions above, we find an analytical closed-form expression for the expected efficiency of a reciprocity-based beamformer PG_{R} suffering from synchronization losses

$$PG_{\text{R}} = \frac{\mathbb{E}\left\{\left|\boldsymbol{h}^{\mathsf{T}}\boldsymbol{s}\right|^2\right\}}{P_{\text{tx}}} = \frac{1}{\|\boldsymbol{h}\|^2}\left(\|\boldsymbol{h}\|_4^4 + \underbrace{2\binom{L}{2}}_{\approx L^2} G_{\text{ch}}^2 e^{-\sigma_\varphi^2}\right) \tag{4.3}$$

$$\approx \begin{cases} \frac{\|\boldsymbol{h}\|_4^4}{\|\boldsymbol{h}\|^2} & \text{Var}\{\varphi_\ell\} > \ln\|\boldsymbol{h}\|^4 - \ln\|\boldsymbol{h}\|_4^4 \quad \dots \text{ low sync. regime} \\ L\,G_{\text{ch}}\,e^{-\sigma_\varphi^2}, & \ln 2 < \text{Var}\{\varphi_\ell\} < \ln\|\boldsymbol{h}\|^4 - \ln\|\boldsymbol{h}\|_4^4 \quad \dots \text{ logarithmic regime} \\ L\,G_{\text{ch}}, & \text{Var}\{\varphi_\ell\} < \ln 2 \quad \dots \text{ high sync. regime} \end{cases} \tag{4.4}$$

which is derived in (A.3) in Appendix A.

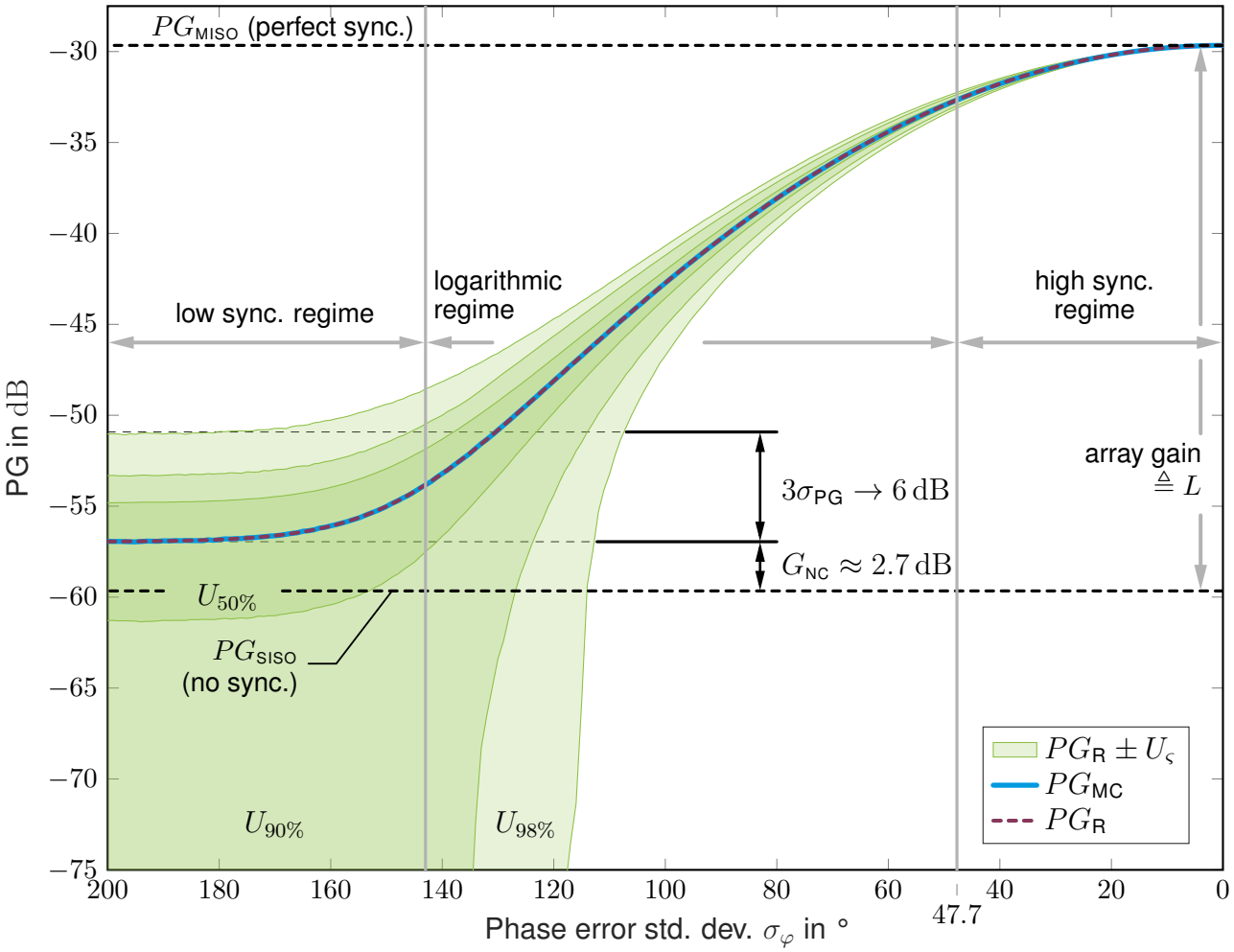

Figure 4.1: Efficiency of a reciprocity-based beamformer suffering from phase synchronization errors based on a measured channel vector $\boldsymbol{h}$ (measured with a synthetic aperture measurement testbed described in [11], [27]). The efficiency is evaluated by means of an MC analysis (i.e., PG_{MC}) and the analytical closed-form expression in (4.3) (i.e., PG_{R}) with the respective synchronization regimes in (4.4).

4.1.2.2 Measurement-based performance evaluation

We demonstrate the fundamental performance limits on channel measurements acquired with a vector network analyzer (VNA). We evaluate a MISO system[1] with $L = 1000$ antennas operating at a frequency $f = 3.8\,\text{GHz}$ and an EN device at a distance of $\|\boldsymbol{r}\| \approx 12.3\,\text{m}$. We evaluate the system efficiency on a measured channel vector $\boldsymbol{h}$, which we assume is the "true"[2] channel, given that we have a reasonably high measurement SNR. Figure 4.1 shows the efficiency of a reciprocity-based beamformer that has perfect CSI (i.e., the measured channel vector $\boldsymbol{h}$) but suffers from the phase errors described in (4.2). The analytical expression in (4.3) is evaluated and compared against a Monte Carlo (MC) analysis with $M = 10^5$ realizations of (4.2), denoted PG_{MC}, times all L antennas, where both curves show a good correspondence. Furthermore, the mean PG_{MC} of the distribution is augmented by symmetric confidence intervals U_{ς} for which one random realization of PG is located within the interval $\left(PG_{\text{R}} - U_{\varsigma},\ PG_{\text{R}} + U_{\varsigma}\right)$ with a confidence

[1] Please refer to [27] for more information on the measurement scenario.

[2] We make this assumption knowing that the "true" value of a measurand is generally unknown and our corrected measurement result is merely its best estimate [28].

level ς, i.e., the probability

$$\varsigma = \mathbb{P}\{PG_{\mathsf{R}} - U_\varsigma \leq PG \leq PG_{\mathsf{R}} + U_\varsigma\}\,. \tag{4.5}$$

Figure 4.1 shows the intervals $\left(PG_{\mathsf{R}} - U_\varsigma,\, PG_{\mathsf{R}} + U_\varsigma\right)$ computed for the confidence levels $\varsigma \in \{50\,\%, 90\,\%, 98\,\%\}$ based on the M realizations from the MC analysis.
The performance characteristic can be divided in the three synchronization regimes described in (4.4):

The *low synchronization regime* is dominated by a non-coherent operation and the array acts as a "stochastic" beamformer. In [27], we show that a beamformer with random weights that are circularly-symmetric complex Gaussian, i.e., $\boldsymbol{w}$ exhibits random phases $[\boldsymbol{w}]_\ell \sim \mathcal{CN}(0, \sigma_w^2)$ where $\|\boldsymbol{w}\| = 1$, has an expected mean path gain PG_{SISO} corresponding to an equivalent SISO system. Interestingly, a non-coherent operation of the array, i.e., exhibiting random phases $\angle[\boldsymbol{w}]_\ell \sim \mathcal{N}(0, \sigma_\varphi^2)$ but deterministic amplitudes $|[\boldsymbol{w}]_\ell| = |[\boldsymbol{h}]_\ell| / \|\boldsymbol{h}\|$, still holds a gain of $G_{\mathsf{NC}} \approx 2.7\,\mathrm{dB}$ compared to PG_{SISO} in the case of a perfectly known channel vector $\boldsymbol{h}$. To express this gain analytically, we rearrange the term for PG_{R} in the low synchronization regime in (4.4) as

$$PG_{\mathsf{R}} \approx \frac{\|\boldsymbol{h}\|_4^4}{\|\boldsymbol{h}\|^2} = \frac{\|\boldsymbol{h}\|_4^4}{\frac{1}{L}\|\boldsymbol{h}\|^4} \underbrace{\frac{1}{L}\|\boldsymbol{h}\|^2}_{=G_{\mathrm{ch}} \approx PG_{\mathsf{SISO}}} \approx \frac{\frac{1}{L}\sum_\ell |[h]_\ell|^4}{\left(\frac{1}{L}\sum_\ell |[h]_\ell|^2\right)^2} PG_{\mathsf{SISO}} \tag{4.6}$$

$$= \left(\frac{\mu_{G_{\mathrm{ch}}}^2 + \sigma_{G_{\mathrm{ch}}}^2}{\mu_{G_{\mathrm{ch}}}^2}\right) PG_{\mathsf{SISO}} \tag{4.7}$$

where we define the sample mean $\mu_{G_{\mathrm{ch}}} = \frac{1}{L}\sum_\ell |[h]_\ell|^2$, corresponding to the 1^{st} sample *raw* moment of the SISO channel power gains $|[h]_\ell|^2$, and the biased sample variance $\sigma_{G_{\mathrm{ch}}}^2 = \frac{1}{L}\sum_\ell \left(|[h]_\ell|^2 - \mu_{G_{\mathrm{ch}}}\right)^2$, corresponding to the 2^{nd} sample *central* moment of the SISO channel power gains. This allows to express the first term in (4.7) by means of the *coefficient of variation* $c_{\mathrm{v}} = \frac{\sigma_{G_{\mathrm{ch}}}}{\mu_{G_{\mathrm{ch}}}}$, which then corresponds to the *non-coherent gain* through

$$G_{\mathsf{NC}} \approx 1 + c_{\mathrm{v}}^2\,. \tag{4.8}$$

Note that the coefficient of variation c_{v} is a measure for the dispersion of the channel power distribution of all L channels from an RW to an EN device. It attains $c_{\mathrm{v}} = 0$, i.e., no gain over a SISO system, for $|[h]_\ell|^2 = |[h]_\jmath|^2\ \forall\ \ell, \jmath \in \{1\ \ldots L\}$. Consequently, in a distributed architecture with some arrays being closer to the EN device than others, the coefficient of variation c_{v} is higher than in the case of using only a single array. As indicated in the figure, *random beamforming*, sometimes also termed *opportunistic beamforming*, may achieve another efficiency improvement of $6\,\mathrm{dB}$ on top of G_{NC} within the 3σ-intervals (capturing approx. $98\,\%$ of the weight realizations, and thus coinciding with the $PG_{\mathsf{R}} \pm U_{98\%}$ confidence interval.). In this regime, the PG is chi-squared distributed and σ denotes its standard deviation (please refer to [20, Appendix C] for more details on the $n\sigma$-intervals). We have found that this gain is also available in the case of circularly-symmetric complex Gaussian weight realizations, in contrast to G_{NC} [27]. Targeting higher gains will be practically unreasonable for most applications due to the large number of weight realizations involved. The amplitudes $|y|$ are approximately Rayleigh-distributed in this regime.

As the synchronization improves, PG_{R} enters a regime of *logarithmic* increase with the phase error variance $\mathrm{Var}\{\varphi_\ell\}$, where the amplitudes $|y|$ are approximately Gaussian. In this transition region from a "stochastic" beamformer to a deterministic beamformer, the relative width of the

confidence intervals $\left(\frac{PG_{\mathsf{R}}-U_{\varsigma}}{PG_{\mathsf{R}}}, \frac{PG_{\mathsf{R}}+U_{\varsigma}}{PG_{\mathsf{R}}}\right)$ of the reciprocity-based beamformer likewise decrease with improving phase synchronization.

Entering the *high synchronization regime*, PG_{R} saturates at the MISO path gain PG_{MISO} requiring both perfect CSI and perfect phase synchronization, and leveraging the full array gain $G_{\mathrm{array}} = L$. Unless operating in the low synchronization regime, the *synchronization power loss* (actually a gain) can be approximated as

$$G_{\mathsf{SYNC}} \approx e^{-\sigma_{\varphi}^2}. \tag{4.9}$$

The REINDEER consortium recommends having a synchronization with a maximum phase error standard deviation of $\sigma_{\varphi} < \sqrt{\ln 2} \approx 47.7°$, which corresponds to an expected power loss (gain) of $G_{\mathsf{SYNC}} \approx -3\,\mathrm{dB}$ with respect to perfect phase coherency. Achieving $G_{\mathsf{SYNC}} > 90\,\%$ and thus $\sigma_{\varphi} < \sqrt{-\ln 0.9} \approx 18.6°$ could be a targetted technical specification for many hardware implementations.

4.1.3 Accuracy of reciprocity assumptions and calibration

A known challenge in mMIMO operating in TDD whereby downlink transmission is with CSI acquired based on uplink pilots, is the need to cope with non-reciprocity of RF front-ends. Indeed while the radio propagation itself and the antennas can be considered reciprocal in downlink and uplink when transmitting over the same frequency band, this can not be said for the multiple transceiver front-ends operating in either receive or transmit in uplink and downlink. The structure of the problem allows the non-reciprocity to be resolved at the access infrastructure side by calibration techniques. The problem has been clarified and potential solutions were originally proposed for conventional multiple-input multiple-output (MIMO) [29]. For mMIMO communications, calibration processes clearly can become much more tedious because of the high number of antennas, yet previous research has shown that the specifications can become more relaxed [30]. Several solutions to implement non-reciprocity calibration have been proposed in literature for central arrays, e.g., by Vieira and co-authors [31], and for distributed topologies [32]. In the frame of REINDEER, over-the-air reciprocity calibration procedures have been extended to distributed panels of antenna arrays [33], i.e. reciprocity calibration of CSPs in the RW concept, based on a joint beam scanning procedure, executed by all CSPs, to collect measurements for the calibration. These REINDEER results will be included in the upcoming D3.2 [34].

For the case of reciprocity based WPT, the corresponding reciprocity calibration procedure depends on whether the same transmit chains in CSPs are used both for communication/positioning and WPT, or if a separate set of transmit chains are needed to achieve high-enough WPT efficiency. In the former case, the reciprocity calibration process for the purpose of communication/positioning can be reused, without additional CSP complexity. In the latter case, where separate transmit chains are used for WPT, an additional but lower-accuracy, reciprocity calibration procedure is needed in the CSPs. This is a consequence of, as elaborated on in Section 4.1.2, the relatively low requirement on phase accuracy for WPT, compared e.g. to the requirements for complex waveforms in high-rate communications. We also expect devices relying on WPT for their operation to have lower requirements on latency introduced by any necessary calibration process to be performed, relaxing requirements on reciprocity calibration for WPT even further. The details of these requirements are subject for future studies.

4.2 Exposure limits and regulations

The European regulations on radiated power and duty cycle limitations were discussed in detail in D4.1. A summary of the guidelines for the major bands considered for WPT is provided here, as we relate them to the assessment made for the infrastructure output requirements derived in the previous chapters of this deliverable.

Table 4.1 summarizes the exposure limits imposed by regulations for different frequency bands. We note hereby that it is not straightforward to interpret the regulatory framework in the context of transmission from many points in a distributed architecture. In the most strict sense, one could state that the overall transmit power and duty cycle from cooperating CSPs should comply with the regulations. Considering the regulations as imposing limitations per transmitter, one could conclude that all CSPs are individually allowed to transmit up to the levels and duty cycles listed in Table 4.1. With coherent operation for the use cases and deployment scenarios considered in REINDEER, the most strict interpretation of regulations can be adhered to. Clearly the more relaxed interpretation would open up possibilities to increase the range of WPT in a RadioWeaves environment significantly, and/or allow many more devices to be served.

Of course, in any case, it remains vital to respect safety limits. The International Commission on Non-Ionizing Radiation Protection (ICNIRP) defines guidelines for limiting exposure to electromagnetic fields [35], clarifying the amount of permissible EMF absorbed by the body skin from EM waves with frequencies 100 kHz to 300 GHz.

Table 4.1: Overview regulatory standards for (e.i.r.p.) levels $> 20\,\mathrm{dBm}$ for ISM bands 0.9, 2.4 and 5 GHz

Start freq. (MHz)	Stop freq. (MHz)	Bandwidth (MHz)	Device category	Max. power (mW)	Duty cycle
865	868	3	Radio Frequency Identification (RFID) devices	2000 (e.r.p.)	Polite access only
865	868	3	Non-specific short-range devices	500 (e.r.p.), APC or comparable	Polite access, and $\leq 10\,\%$ for network access points $\leq 2.5\,\%$ otherwise
869.4	869.65	0.25	Non-specific short-range devices	500 (e.r.p.)	Polite access, or $\leq 10\,\%$
874	874.4	0.4	Non-specific short-range devices	500 (e.r.p.), APC or comparable	Polite access, and $\leq 10\,\%$ for network access points $\leq 2.5\,\%$ otherwise
916.1	918.9	2.8	Radio Frequency Identification (RFID) devices	4000 (e.r.p.)	Polite access only
917.3	918.9	1.6	Non-specific short-range devices	500 (e.r.p.), APC or comparable	Polite access, and $\leq 10\,\%$ for network access points $\leq 2.5\,\%$ otherwise
2400	2483.5	83.5	Wideband data transmission devices	100 (e.i.r.p.)	Polite access
2446	2454	8	Radio Frequency Identification (RFID) devices	500 (e.i.r.p.)	Polite access
2446	2454	8	Radio Frequency Identification (RFID) devices	4000 (e.i.r.p.)	Polite acces, or $\leq 15\,\%$ over any $200\,\mathrm{ms}$
5150	5250	100	Wireless Access Systems (WAS)/ Radio Local Area Networks (RLANs)	200 (e.i.r.p.)	Polite access
5250	5350	100	Wireless Access Systems (WAS)/ Radio Local Area Networks (RLANs)	200 (e.i.r.p.)	Polite access
5470	5725	255	Wireless Access Systems (WAS)/ Radio Local Area Networks (RLANs)	1000 (e.i.r.p.)	Polite access
5725	5875	150	Wireless Industrial Applications (WIA)	400 (e.i.r.p.)	Polite access

Chapter 5

Contact service point hardware requirements for WPT

This assessment describes the specific hardware requirements at the infrastructure side to provide energy to the EN and potentially backscattering nodes. This chapter refers back to Section 3.1 and discusses hardware related challenges and requirements specifically for wireless power transfer and not for communication, localisation, etc, of course with the understanding that the transferred energy may be used at the EN side communication or positioning purposes.

5.1 Options to implement the CSP architecture

Several architectural proposals are suggested for the implementation of the channel estimation (CE) of the CSP, in particular focusing on the RF front-end. Given the typical low complexity of the digital baseband and control with respect to communication and positioning functionalities, it is assumed that available resources for the latter could be reused for WPT.

The final decision on which RF front-end architecture to implement will depend on the use case specifications and potential trade-offs between performance, e.g., in terms of number of EN nodes that can be served, and hardware complexity. This section discusses the more complex architecture to enable coherent operation by multiple CSPs resulting in a highly efficient energy delivery solution, which is a main benefit arising from the distributed architecture with many radios. Moreover, the RF front-end components for SISO or non-coherent operation systems are also discussed, showing that the complexity could be significantly reduced yet consequently providing lower performance values as was explained in Chapter 3.

5.1.1 CSP transmit RF front-end without synchronization capabilities

The options 1, 2 and 3 described in Section 3.1, do not require hardware components for synchronization. In these cases, one or more low-complexity CSP implementations suffice to support RF energy transfer. Figure 5.1 shows basic RF front-end architectures which are sufficient to support SISO and non-coherent energy transfer. The baseband signal could also consist of a multi-sine signal to generate a high-PAPR signal. This could ensure energy gains in the RF-DC conversion of the harvester, as discussed in Section 3.3.3. The transmit waveform then consists of frequency components that are upconverted by the local oscillator (LO) and the mixer. On the contrary, a

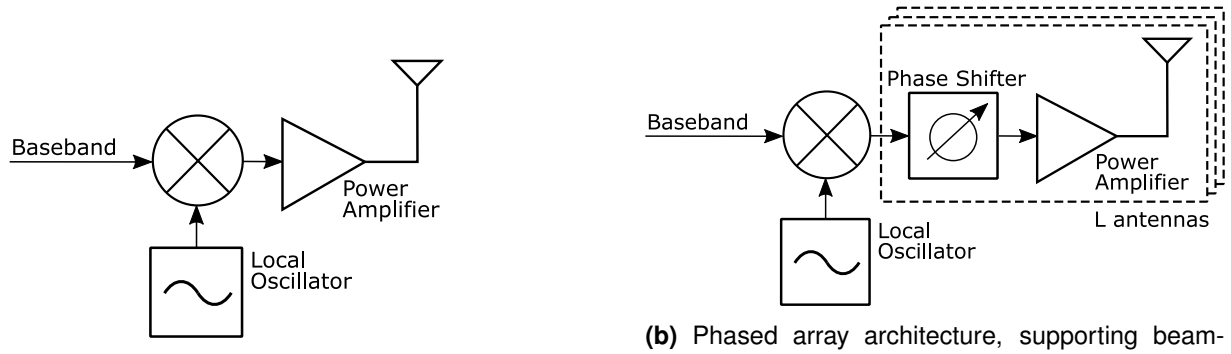

(a) Low complex representation for SISO systems.

(b) Phased array architecture, supporting beamforming capabilities.

Figure 5.1: Basic RF front-end architecture.

constant frequency baseband signal will produce a single tone signal f_{lo} after mixing. Actually, in the most basic implementation with single tone signals, even the mixer could be removed as for SISO or non coherent wireless power transfer only an amplified single-tone RF signal is required. To further support beamforming, a phase shifter can be added between the mixer and the PA to construct phased arrays, shown in Figure 5.1b.

Several challenges are associated with supporting multi-band signals. On the one side, there is need for wide-band antennas, briefly discussed in Section 5.2.1. Generating such signals can be done, for example, by equipping the RF front-end as in Figure 5.1a with multiple LOs, mixers and phase shifters that then go through an RF combiner and a wide-band PA. The amplified multi-band signal must then be radiated through an associated multi-band antenna. In previous deliverables, it was mentioned that the Reindeer project considered four frequency bands ($868\,\mathrm{MHz}$, $2.4\,\mathrm{GHz}$, $3.7\,\mathrm{GHz}$ and $5\,\mathrm{GHz}$). Therefore, the RF front end hardware should be suitable to operate in these frequency bands.

5.1.2 CSP architecture for coherent WPT in RadioWeaves infrastructure

The fourth option discussed in Section 3.1 considers a RadioWeaves infrastructure with multiple distributed CSPs that coherently operate and serve the EN device with RF power. The signals generated by multiple CSPs create a power spot around the EN device. In this section, the minimum hardware requirements to only generate power spots at the EN device locations are explored. No hardware for communication, localization or other functions are discussed here. The CSP hardware for two implementation options will be discussion further: distributed beamforming via MRT and a closed loop approach.

5.1.2.1 Distributed beamforming via MRT - local open loop approach

Assume the EN device location is known and the channel response is estimated, then Figure 5.2 illustrates the minimal hardware components to create power spots via MRT. This open loop approach refers to the CSP itself. The whole implementation with central processing units, X-haul communication links and CSPs can be represented in fact as a globally closed loop system where each openenly communicating CSP system requires information from the centrals processing unit.

By supplying a distributed input reference clock without frequency offset and drift to the individual PLLs, the desired stable RF frequencies on each CSP can be generated. If the registers of all

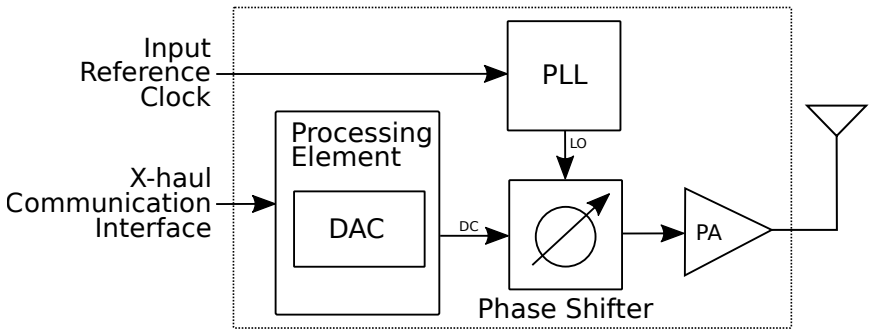

Figure 5.2: Minimal RF front end components to generate power spot. This analog implementation is the most basic and low cost CSP architecture to support beamspots at the desired location.

PLLs are set to the same values, then all LO signals should have the same output frequency. The PLL may not cause any unwanted phase offsets so that all LO signals can be assumed phase coherent. Therefore, a phase coherent PLL implementation is required and further explained in Section 5.2.3.

The processing element (PE) gets phase information through the X-haul communication interface from the edge computing service point (ECSP). The digital-to-analog converter (DAC), embedded in the PE, outputs a DC voltage that is mixed with the LO signal. After amplification, the amplified phase shifted signal is radiated via the antenna to the EN device.

A digital alternative for the analog baseband implementation from Figure 5.2, can be obtained by replacing the phase shifter by a mixer. Unlike a DC output voltage generated by the the PE, a baseband signal could then be fed to the input of the mixer, making the architecture also usable for communication. To accomplish baseband transmission, the DAC will generate samples at a certain frequency. Consequently, an additional low-pass filter (LPF) behind the DAC and before the mixer is recommended in such an architecture, further complicating it.

5.1.2.2 Locally closed loop approach

This approach is explained more extensively in D4.2. The minimum hardware required to support this approach is explained here. In short, predefined reference signals, called pilots, are transmitted or backscattered by the EN device and received by several CSPs. Via these signals, the CSP does not need any channel information as it can easily rebroadcast the same signal. Via these uplink pilot messages the CSPs have enough information through the involved receivers to regenerate a power spot around the EN device, meaning that the transmitted signal should have a similar phase shift as the incoming pilot signal.

Figure 5.3 shows the minimal CSP requirements to support the closed loop approach. One transceiver antenna is proposed. This implementation assumes a half duplex front-end system. An RF switch distinguishes the RX chain from the TX chain.

The pilot signal is received by the transceiver antenna and redirected to the RX chain. The low power signal is first amplified through a low noise amplifier (LNA) and then compared to the LO through the phase detector. The phase detector is actually a mixer generating two signal components $f_{in} - f_{lo}$ and $f_{in} + f_{lo}$ as output. The PLL is assumed to be set at the same frequency as the backscattered signal. This means that $f_{in} = f_{lo}$. The output of the phase detector will generate a sine signal with only one frequency component $2 \cdot f_{in}$ and a DC offset. The latter represents the phase between local oscillator and input signal. After filtering the phase detector

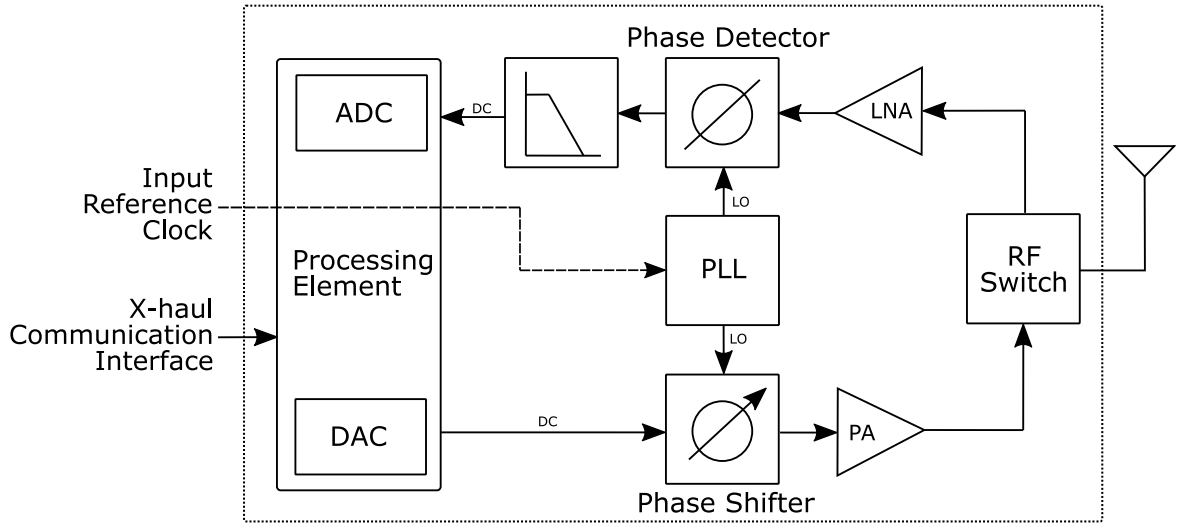

Figure 5.3: Minimal CSP architectural hardware requirements to support the closed loop approach.

output, only the DC offset remains and is forwarded to the embedded analog-to-digital converter (ADC) of the PE. The reverse principle is valid by using the DAC to generate the same DC voltage and thus same phase offset against the reference signal. Here the PE actually serves as a kind of buffer to store the DC voltage obtained during the pilot transmission. The RF switch can now be connected to the PA of the TX chain. The DAC can generate the desired voltage that will ensure a phase shifted signal. Note, that the RX and TX chain should have similar behavior. The phase offsets coming from TX and RX paths and components should be equal. Section 4.1.3 handles this requirement and reciprocity calibration.

Lets us assume each CSP has a reference clock without frequency offset and drift. A phase synchronized mechanism is not required since it only servers as a reference clock for the receiver and the transmitter front-end. Thus, there is no need for a phase coherent PLL. The PLL is further discussed in Section 5.2.3. The most important requirement is to have a stable clock which is not drifting in time. Strict time synchronisation is also not required. This simplified representation assumes only single tone signals to be re-transmitted. High-PAPR signals require more complex hardware and are left out of the scope of this discussion on CSP hardware requirements. Moreover, the CSP depicted here has only one antenna. However, the PE may serve multiple similar RF front-ends in one CSP to drive multiple antennas simultaneously.

In essence, the CSP hardware must be able to measure the phase of the pilot signals with respect to the internal LO. Furthermore, a phase offset must be added to the LO to re-radiate the same signal and generate a power spot at the desired location. Other hardware implementations than the one proposed here are possible, for example to increase the flexibility of the hardware to also allowing communication or support multi-band operation.

The schematic represented in Figure 5.3 illustrates the analog solution for the closed loop approach. An alternative implementation could be realized based on a digital baseband signal, for which the phase detector and phase shifter can be replaced by a mixer to upconvert the baseband signals while still managing the desired phase. The result is then a CSP architecture that allows communication by radiating baseband signals generated by the PE and alternating provide energy to the EN device.

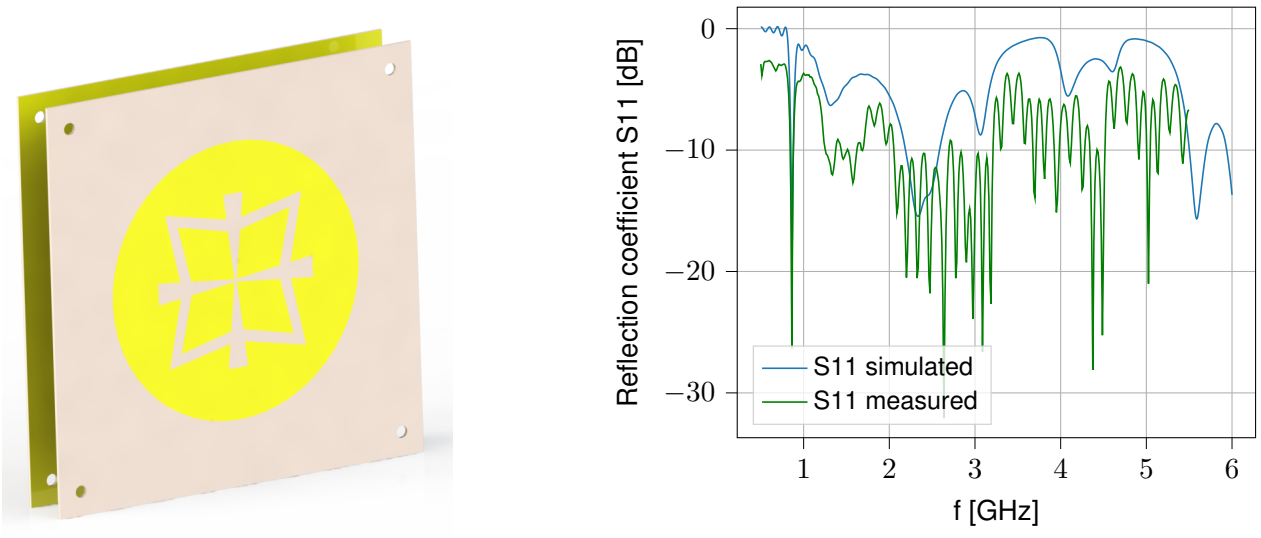

(a) Antenna render.

(b) Reflection coefficient.

Figure 5.4: Low cost multi-band antenna design.

5.2 Analysis of the individual components

In this section we list the critical hardware components of the CSP for WPT purposes, in particular realting to the antenna and RF front-end, and discuss them briefly.

5.2.1 Low cost antennas

The choice of the antenna will highly depend on the use case, deployment scenario and expected EN device locations. The implementation example of Figure 2.4 showed that the patch-antenna for this scenario provides the best performance and efficiency. The design of the antenna should be consistent with the operating conditions so that the maximum benefit of antenna gain is achieved and polarization losses are minimized.

A reasonably small bandwidth for the REs is sufficient to support wireless power at the infrastructure side. No communication is necessary and in view of hardware complexity, we assume only a single frequency component to be radiated. In exceptional cases, high-PAPR signals can be considered, as discussed in Section 3.3.3. For example, a multi-sine signal can be radiated with limited antenna bandwidth, meaning a couple of MHz should already suffice.

The harvested energy per unit time can be increased by implementing a multi-band harvester in the EN device as discussed in Section 3.3.2. Regulatory constraints can be overcome to some extent by combining multiple frequency bands, each with their limitations, using this approach. The antenna presented in Figure 5.4 can be widely used. This antenna can transmit and receive in the $868\,\mathrm{MHz}$, $2.4\,\mathrm{GHz}$ and $5\,\mathrm{GHz}$ bands.

Section 6.2 investigate the trade-off between the antenna gain and the backscattering range for different use cases. The parameters antenna gain and obviously operating frequency partially determine the antenna dimensions. Consequently, bigger antenna elements will affects the unit price.

5.2.2 Power amplifiers

The PA is a major contributor to the power consumption in a WPT system. It should first of all generate the power to be radiated to the antenna. Moreover, depending on the waveform to be transmitted, it should demonstrate a linear behavior in a certain range. However, a high dynamic range typically comes with a low efficiency, as this will require the PA to operate in a point backing off from the most efficient zone, which is near it's saturation. The linearity requirement and the target to provide the highest possible efficiency will be the main factors in decision on which class of amplifier to select for the PA. We here below discuss key parameters to be taken into account when selecting a PA, relate these to the specifications for WPT, and comment on the suitability of different classes of PAs from that perspective.

The DC to RF efficiency of the WPT transmit process is determined by dividing the radiated RF power by the consumption of the components from Figures 5.1 to 5.3 that generate and amplify the desired signals. In the CSP, much of the power will be lost in the PA operation, and hence it is of key importance to select a suitable technology.

The PA's main task is amplifying the signals coming from the phase shifter or mixer to the desired RMS voltage level, so that the desired power in $[\mathrm{dBm}]$ is radiated at a matched impedance of $50\,\Omega$. The maximum power required by a certain use case, will clearly impact the PA technology selection. A distinction between switched mode PAs and linear PAs is often made. More about the types and classes is explained in detail in [36], [37]. The class-A PA corresponds most closely to an ideal linear amplifier. Its main drawback is the typically low efficiency of $< 50\,\%$.

Continuing with the specifications, the PA bandwidth can be rather small for the signals to be radiated to support the energy transfer, especially if only single tone signals are considered. Even for high PAPR signals, generated by multi-sine signals, a bandwidth of only a couple of MHz is sufficient. Distortions, introduced by the amplifier, are better avoided since these can cause the power to get dispersed over multiple spectral components, resulting in efficiency drops of the WPT over the link. Consequently, the harvester efficiency will be lower than expected, e.g., if the signal is not proportionally amplified, as can happen by a clipping signal in the PA. However, when considering total energy consumption operating a PA close to saturation in a non-linear region, can be most efficient. The impact of non-linear distortions in distributed mMIMO is more comprehensively discussed in Section 5.3. In addition, the PA should not introduce any arbitrary phase shift or at least any occurring offsets should be measured and eliminated, since this would cause a significant problem in (distributed) beamforming as is required for a RadioWeaves system.

Simulations that carefully simulate the room and use case, provide an approximation of the required transmit power each individual RE element. Consequently, these results help to select the most appropriate PA technology. In Table 3.3 from Chapter 3, this was calculated for the ESL use case for coherent operation. From this analysis it is concluded that a transmit power per individual antenna less than $10\,\mathrm{dBm}$ is required, which corresponds to only $10\,\mathrm{mW}$ of RF power. Very low cost PAs, such as a Monolithic Amplifier [38], can suffice. With only one IC and some matching components, this PA circuitry is complete. Higher efficiency can be obtained by selecting switched mode PAs. Class E amplifiers are designed to achieve high efficiency levels and are perfectly suitable for operation in the UHF band. The latter more complex design serves extremely high efficiencies. E.g. in [37] Figure 7.18 (page 211), a class E amplifier is reported achieving an efficiency of $87\,\%$ for $31.7\,\mathrm{dBm}$ output power. Beside the efficiency, the bandwidth of these PAs can be very broad [39], [40], which make these amplifiers very good candidates for RF-WPT in RadioWeaves. Any occurring phase offset due to class E PAs can be resolved in

reciprocity calibration mentioned in Section 4.1.3.

High PAPR signals need to be supported in basestations for 4G and 5G networks. This requires PAs with a linear response and a high dynamic range. Conventional architectures such as class A amplifiers will in these circumstances operate at low efficiency. The efficiency of PAs can be improved with envelope tracking or Doherty techniques [36]. Similar techniques could be considered to improve the DC-RF efficiency of the CSPs in the RadioWeaves architecture. A Doherty transmitter is implemented with one main PA and an auxiliary PA. The latter is accessed during peaks in the signal [36]. However, the expected power levels related to the considered use cases (D1.1) are relatively low compared to the required power levels in macro base stations, and notably the PAPR of the signals will not be high and an efficient operation point can be established. We expect only marginal energy gains by implementing Doherty amplifiers and consequently the design complexity and cost will unnecessarily increase. The designer could make a trade off between complexity of the amplification hardware and the power consumption.

As an example, a commercially available highly efficient single channel CMOS power amplifier [41] for RF-based WPT is proposed by Energoues.

5.2.3 Phase-locked loop

A PLL is usually necessary to generate the desired RF signal from an input reference signal. Even with direct RF sampling, the reference signal may be lower than all the clocks. Because of the crucial role and the requirement to have a good knowledge of the all clocks, frequency synthesizers and their main shortcomings and features are analyzed in this section.

The classical N-integer PLL integration transforms a reference frequency F_r to a higher output frequency F_{vco}. The ratio is denoted by N such that $F_{vco} = N \cdot F_r$. F_{vco}/N is compared to F_r by the phase detector. In case of frequency difference, the voltage at the voltage-controlled oscillator (VCO) is adjusted, so that F_{VCO}/N is locked at the reference frequency. By modifying the divider N, the output frequency can be adjusted. The basic schematic is shown in Figure 5.5 [42].

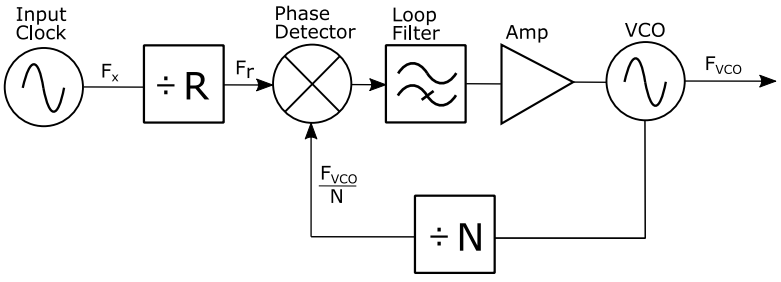

Figure 5.5: Basic PLL scheme [42].

Often a clock input source F_X, for example, from a temperature compensated crystal oscillator (TCXO) is divided by R, giving F_r. The output frequency related to the reference frequency can be calculated via Equation (5.1). A TCXO, as input source, can provide higher frequency stability, lower than $1\,\mathrm{ppm}$ and is often selected. The frequency stability of F_{vco} will be equal to the stability of the input frequency source (e.g., if selected, the TCXO stability).

$$F_r = \frac{F_X}{R} = \frac{F_{VCO}}{N} \tag{5.1}$$

The spacing between the discrete frequency components that can be generated, called channel spacing, is represented by F_r. For an integer-N PLL, the phase detectors are running at the reference frequency, which equals the channel spacing frequency. F_r consequently also corresponds to the frequency resolution. A smaller channel spacing F_r logically results in a more accurately adjustable output frequency, with the consequence that the frequency multiplication N should become large to achieve the same output F_{vco}. Unfortunately, the phase noise depends on N and is given by $20\log(N)$ [42]. The phase detectors are responsible for close-in phase noise, which means the phase noise close to the carrier frequency. For example, for N equal to 10000, the phase noise will be $80\,\mathrm{dB}$ worse.

After the phase detector, typically a loop filter is placed. The purpose is to reduce the harmonics or spurious signals around the reference frequency $\pm F_r$. To reduce the spurious signals as much as possible, it is best to select a narrow bandwidth for the loop filter. However, a narrower bandwidth increases the time to switch between channels. If N could be reduced, F_r can increase and as a consequence the loop filter bandwidth may increase, so a smaller switching time T_{SW} is obtained [42]. Since RF wireless power transfer does not require rapid switching between frequency channels, this PLL integration is sufficient.

A more recent PLL technology allows the phase detector frequency to be increased without sacrificing synthesizer channel spacing or frequency resolution. With a fractional-N PLL, the frequency resolution can be set as a fraction F of the phase detector frequency. This is done by dynamically adapting the divider, from Figure 5.5, between N and $N+1$. The average divider ratio is given by K/F where K, represents the fractional channel of operation and F represents the fractional resolution or modulus. To accomplish this, the low complex division circuit (ensuring the division N from Equation (5.1)), is replaced by the fractional accumulator. The implementation details of the fractional accumulator are out the scope of this discussion. Equation (5.2) represents the F_{vco} of a fractional-N frequency synthesizer.

$$F_{VCO} = F_r \cdot \left(N + \frac{K}{F}\right) \tag{5.2}$$

Generating output signals with PLLs could results in synchronisation issues, even while using the same reference clock. More specifically, phase offsets can occure and should be controlled accurately during the selection of the PLL architecture. In the reindeer project perfectly synchronized signals are crucial to support several use cases in a distributed architecture. Further analysis in this section looks at the PLL synchronisation issues and how they can be solved.

5.2.3.1 Frequency drift/offset

We first assess the frequency drift and offset impact by the PLL. As already mentioned, the frequency stability of the PLL output signal depends on the stability of the input clock. Since the PLL circuit does not change the frequency stability, the reference clock, available on each CSP, should be perfectly synchronized (explained in D2.2 [26]). Suppose a reference clock, with accurate frequency stability, is distributed to all CSP devices, then a frequency drift cannot occur. Similarly, since the same clock is routed to all CSPs, frequency offset cannot occur.

5.2.3.2 Phase drift/offset

A phase drift can occur due to a frequency offset or drift between two reference signals of two individual PLLs. This logically will not create a constant phase neither a coherent phase relation

between the output signals of the PLLs. However, even for phase coherent reference signals, the PLL can introduce phase offsets, which leads to problems, for example, in distributed beamforming to correctly steer the phased-array antennas. Suppose the same reference signal is connected with two individual PLLs and they are both set to the same multiplication factor N. Then both PLLs will lock at the desired output frequency. Furthermore, a phase lock will occur on both PLLs. However, a phase difference between the output signals of both PLLs may occur and can vary between zero and one period. It may be noted, that the phase does not drift and remains constant in time. Since this phase offset is unwanted, its occurrence of these phase offsets must be controlled and eliminated.

5.2.3.3 Phase coherent PLLs

According to [43], phase coherency can be achieved with an N-integer PLL. The same reference clock is required on the one hand, and on the other hand, each PLL must be reset at the same time to align the PLL counters to ensure the internal dividers in the PLL start counting from the same start-point.

Conversely, a fractional-N PLL will lock on one of the F phase offsets with respect to the input reference. Relative phase coherency will not occur between the output of multiple fractional-N PLLs. A simple reset signal, as can be done in integer-N PLLs, cannot solve the problem here. We leave the detailed description out the scope of this analysis and refer the reader to [43].

5.2.3.4 Eliminating phase offset

Some fraction-N PLL implementations come with an input pin to enable phase coherency. An example is the LMX2594 [44], which has a SYNC input to synchronize its output with the incoming pulse. With a distributed PPS signal, phase offsets can be eliminated. Another solution is to measure the phase offset by providing a feedback link from the TX RF chain back to the RX RF chain. While keeping the PLL registers and settings, the phase offset will stay constant in time. The unknown offset can be measured first and subsequently eliminated in software. For example, a hardware example with feedback loop between TX and RX chain can be found in the *AD-FMCOMMS5 RF development board*. After measuring the phase offset, the offset can be corrected upon transmission of a new signal. This principle is linked to reciprocity calibration from Section 4.1.3. Limited offsets may still be present and tolerable, as discussed in Section 4.1.2 where the acceptable phase offsets for generating a power spot within a RadioWeaves infrastructure were clarified.

5.3 Out-of-band constraints due to frontend non-linearities

It has been discussed in Section 3.3.3 above considering waveforms that from a perspective of receiving energy at the EN side, the actual hardware circuits often will operate more efficiently with high-PAPR signals. However, these waveforms require a high dynamic range of the PA, resulting in the operation of the PA at a lower efficiency than it's optimal point. The reason for which the PAs is often working in a low-efficient operating point is the fact that PAs demonstrate non-linear behavior when working in their most efficient zone near saturation on the one hand, and the fact that high-PAPR transmission waveforms demonstrate a high dynamic range, and hence require the PA to work with a significant back-off with respect to this most efficient zone, on the other hand. A trade-off between performance and efficiency is hence to be made [45]. Non-linear

distortions result in both in-band signal degradation and out-of-band emissions. The latter are especially problematic as they may result in regulatory violations.
Several authors, including partners in REINDEER, have investigated how non-linear distortion terms may or may not get dispersed or receive antenna gain in massive MIMO systems deploying one central array [46], [47], and distributed massive MIMO systems in particular [48].These analyses show that:

- It is an over-simplification to assume that distortion terms from non-linear PA operation in large array systems are uncorrelated [46].
- In several non-trivial situations, e.g., in transmission to one or few terminals in (predominantly) LoS situations, non-linear distortion terms will combine coherently [49], both in-band and out-of-band. The dynamic range of precoded signals in massive MIMO transmission is often large, which hence requires a significant back-off and inefficient operation of the PAs. Techniques such as digital pre-distortion (DPD) may to some extent improve the efficiency-linearity trade-off [50]. Also, novel precoders have been proposed that prevent coherent combination in space of non-linear distortion terms [51].
- In evolving from transmission from one central large array to distributed massive MIMO antennas and arrays, it is noted that for a system having the same total number of antennas, the distortion in distributed deployments is considerably more uniformly distributed in space. Moreover, the places where potential coherent combination of distortion terms is to be expected, are more contained and can be found in a beamspot around the intended terminal(s) [48].

We consider the above for the case of WPT from CSPs in a RW infrastructure and the question addressed in this deliverable to specify the RW hardware requirements to support energy transfer to energy-neutral nodes. For (multi-user) communication the main performance goal is to maximize signal-to-interference-plus-noise ratio (SNIR). Contrary, for transferring energy to devices one can simplify that the main goal is to maximize the received power, and , e.g., multi-user interference will not be equally detrimental. To maximize the actually amount of energy to be transmitted, if possible CSPs providing a LoS situation to the devices and charging them mostly via the dominant path, will be favorable. In combination with the goal to operate the PA efficiently close to saturation, there is a significant risk that non-linear distortion terms and resulting out-of-band radiation will occur. The following guidelines hence need to be considered in view of optimizing energy efficiency of WPT in the PA stage within regulatory constraints:

1. Waveform and precoding design: from the PA stage perspective, one could favor techniques resulting in (close to) constant envelope per antenna transmission, as for example discussed in [52]. Also, precoders such as proposed in [51] are of interest in particular in the large antenna case, as they allow operating the PAs close to saturation and exhibit an overall energy benefit, while a possible impact in terms of interference does not pose a problem for WPT.
2. The selection of a PA to equip CSPs for WPT may differ from the one for communication purposes, as the latter may require a better linearity and higher dynamic range. A trade-off between hardware reuse for the different functions to be supported at the CSP on the one hand, and energy efficient operation at the other hand, needs to be made. As the RF front-ends for WPT can be low-complexity and in order to achieve a high energy efficiency, it is the working assumption in REINDEER that separate radios will be foreseen for the WPT functionality.

Chapter 6

Backscattering

As little energy is available at EN devices, backscatter communication is considered to transfer information back to the RW infrastructure. Compared to active transceivers, signals are no longer created using powered RF front-ends. In backscattering, incident RF waves from surrounding sources are used as a medium to convey information. While this strategy could should drastically improve power consumption, at the EN side, challenges arise in, among other things, improving the transmission range and separating simultaneously backscattered signals from multiple EN devices. The former challenge is the result of the additional attenuation radio waves experience due to retransmission. The latter problem follows from the often non-existent or limited synchronisation in communication between EN devices given their limited energy budget.

6.1 RF backscattering recap

Deliverable D4.1 [3] initially analyzed the link budget for RF backscattering in a RW environment. As we will continue to build on the concepts and conclusions presented herein, this paragraph will briefly describe the mathematical equations involved in RF backscattering as well as recapitulate on the studies and design choices that have been made earlier on.

When radio waves impinge on an object, a portion of the energy is reflected back to the source. In RF backscatter communication, this scattering property is used to embed information in incident radio waves and convey information wirelessly to a receiver device. The far field parameter used to describe the scattering property of an object is the radar cross section (RCS) σ, is defined in [53] as:

> "a fictive area intercepting that amount of power, which, when scattered isotropically, produces at the receiver a density which is equal to that scattered by the actual target."

A simplified approach is visualized in Figure 6.1, intuitively showing that many parameters will affect the RCS value, such as the relative position of the transmitter, receiver and scatter device, as well as the scatter device's geometry, material and orientation, the radio wave frequency and polarization [54].

Introducing a backscatter device with radar cross section σ into a Friis transmission scenario gives rise to the bistatic radar range equation:

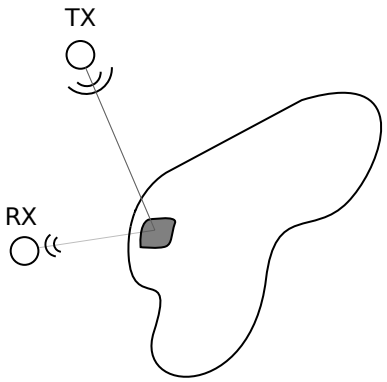

Figure 6.1: Simplified approach of the radar cross section.

$$P_{\mathrm{r,b}} = \sigma \left(1 - |\Gamma_{\mathrm{t}}|^2\right)\left(1 - |\Gamma_{\mathrm{r}}|^2\right)\left(\frac{\lambda}{4\pi d_1 d_2}\right)^2 \frac{P_{\mathrm{t}} G_{\mathrm{t}} G_{\mathrm{r}}}{4\pi} \left|\boldsymbol{\rho}_{\mathrm{t}} \cdot \boldsymbol{\rho}_{\mathrm{b}}\right|^2 \left|\boldsymbol{\rho}_{\mathrm{b}} \cdot \boldsymbol{\rho}_{\mathrm{r}}\right|^2, \tag{6.1}$$

where

- $P_{\mathrm{r,b}}$ is the received power at the receiver side,
- Γ_{t} and Γ_{r} are the reflection coefficients at the input terminals of the transmitter and receiver antenna respectively,
- λ is the signal wavelength,
- d_1 and d_2 are the distances between the transmitter device and the backscatter device, and the backscatter and receiver device respectively,
- P_{t} is the transmit power,
- G_{t} and G_{r} are the antenna gains of transmitter and receiver antenna respectively,
- $\left|\boldsymbol{\rho}_{\mathrm{t}} \cdot \boldsymbol{\rho}_{\mathrm{b}}\right|^2$ and $\left|\boldsymbol{\rho}_{\mathrm{b}} \cdot \boldsymbol{\rho}_{\mathrm{r}}\right|^2$ are representing the polarization mismatch between the transmitter and backscatter device, and the backscatter and receiver device respectively.

The bistatic radar range equation (Eq. 6.1) shows that an EN device is able to transmit information to a receiver by modulating its RCS. Practically, Green [55] presented that the RCS can be altered by changing the antenna load. Connecting two different loads $Z_i, i \in \{1, 2\}$ to the backscatter device's antenna leads to two different reflection coefficients, and consequently a differential RCS $\Delta\sigma$ [56]:

$$\Delta\sigma = \frac{\lambda^2 G_b^2}{4\pi} \left|\Gamma_{b,0} - \Gamma_{b,1}\right|, \tag{6.2}$$

where G_b is the gain of the backscatter antenna and $\Gamma_{\mathrm{b},i}$ is the antenna mode of the backscatter antenna for load i. This is only true for minimum scattering antennas, as is elaborated in more detail in Deliverable 4.1 [3].

We identified on-off keying (OOK) as a very suitable modulation technique for uplink data backscattering in Deliverable 4.1 [3]. OOK can be realised through load switching, which is easy to implement, inexpensive and has been proven to work in several wireless technologies [57], [58]. One major drawback of this modulation method, however, is that it is relatively susceptible to noise. The theoretical upper limit on the achievable bit rate $R_{\max}$ for amplitude shift keying (ASK)

backscatter communication was approximated using the Shannon-Hartley theorem:

$$\begin{aligned} R_{\max} &\leq B \log_2(1 + \mathrm{SNR}) \\ &\leq B \log_2(1 + \frac{P_{\mathrm{signal}}}{P_{\mathrm{noise}}}), \end{aligned} \tag{6.3}$$

where B is the bandwidth of the backscatter channel, SNR is the signal-to-noise ratio, P_{signal} is the average signal power over the bandwidth B and P_{noise} is the average noise power over the bandwidth B.

In the presented setup, P_{signal} is attributed to the differential received backscatter signal coming from the backscatter device $\Delta P_{\mathrm{r,b}}$ which can be obtained by introducing the differential RCS from Equation (6.2) in Equation (6.1). We consider perfectly tuned antennas and no polarization losses.

$$\Delta P_{\mathrm{r,b}} = P_{\mathrm{t}}\, \Delta\sigma\, \frac{\lambda^2\, G_{\mathrm{t}}\, G_{\mathrm{r}}}{(4\pi)^3\, d_1^2\, d_2^2}\,. \tag{6.4}$$

If the backscattered signal can be filtered out perfectly, for example by using a local oscillator, we only need to take into account the AWGN channel assumed by the Shannon-Hartley theorem for P_{noise}. The latter is determined by the noise figure NF of the used hardware, the bandwidth B and the noise power density N_0, in its term function of the temperature T and Boltzmann constant k.

$$P_{\mathrm{noise}} = 10 \log_{10}\left(kT\, \frac{\mathrm{Hz}}{1\,\mathrm{mW}}\right) + NF + 10 \log_{10}(B) \tag{6.5}$$

Consequently, the Shannon-Hartley equation for the considered backscattering system becomes:

$$\begin{aligned} R_{\max} &\leq B \cdot \log_2\left(1 + \mathrm{SNR}\right) \\ &\leq B \cdot \log_2\left(1 + \frac{P_{\mathrm{t}}\, \Delta\sigma\, \frac{\lambda^2\, G_{\mathrm{t}}\, G_{\mathrm{r}}}{(4\pi)^3\, d_1^2\, d_2^2}}{P_{\mathrm{noise}}}\right). \end{aligned} \tag{6.6}$$

If we consider a MISO system where several transmitters work together, we have to account for the additional array gain G_{array}:

$$R_{\max} \leq B \cdot \log_2\left(1 + \frac{P_{\mathrm{t}}\, \Delta\sigma\, \frac{\lambda^2\, G_{\mathrm{t}}\, G_{\mathrm{r}} G_{\mathrm{array}}}{(4\pi)^3\, d_1^2\, d_2^2}}{P_{\mathrm{noise}}}\right). \tag{6.7}$$

6.2 Extend transmission range

Communication range plays a crucial role in the applicability of RF backscattering in many use cases, and consequently for the feasibility of EN devices. However, as radio waves get significantly attenuated after backscattering, the communication distance is negatively affected. In this regard, RW brings the advantage of many radio elements. On the one hand, transmitter and receivers can be allocated closer to the backscattering device, minimizing distance. On the other

hand, multiple radio elements can cooperate to create larger apertures, compensating for the larger distances. This section investigates the infrastructure resources needed in a RW environment to allow for backscattering over large distances. The use cases presented in Deliverable 1.1 [1] serve as a base for this study.

6.2.1 Backscattering communication range

Starting from the adapted Shannon-Hartley equation (Eq. 6.7), we are able to gain insights in the RW and channel resources needed for proper decoding of the backscattered signals at the receiver. The trade-off between the RW and channel parameters on the one side, and the maximum feasible propagation distances between each of the devices becomes clear by isolating d_1 and d_2 in Eq. 6.7. d_1 is the distance between the RW transmitter(s) and the backscatter device, and d_2 is the distance between the backscatter device and the RW receiver(s).

$$(d_1 d_2)^2 \leq \frac{P_{\mathrm{t}} \Delta\sigma \lambda^2 G_{\mathrm{t}} G_{\mathrm{r}} G_{\mathrm{array}}}{(4\pi)^3 (e^{\frac{R_{\max} \ln 2}{B}} - 1) P_{\mathrm{noise}}} \tag{6.8}$$

From Eq. 6.8 it is clear that the RW infrastructure can effectively increase d_1 and/or d_2 by boosting the total transmit power P_{t} and/or allocating more RW transmitters to increase the total array gain G_{array}.

6.2.2 Allocation of RW resources

The backscatter communication range that needs to be covered will be determined by the environment in which the application is running. Equation (6.8) shows that it is in the advantage of the RW infrastructure to keep the distance to the backscattering EN device small as less transmitters and/or readers will have to be allocated to ensure reliable communication. However, multiple applications may need to be served at the same time, with the result that not all RW elements will be available at a certain moment in time. This section investigates how RF resources need to scale in order for RF backscattering to work in realistic scenarios.

In what follows, we assume a MISO backscatter setup, composed of multiple transmitters placed at a distance from the receiver. We also consider true-to-life channel parameters and system components. An overview of these assumptions is listed in Table 6.1. For both the transmitter and receiver antennas we consider λ/2 dipoles with a theoretical gain of $2.15\,\mathrm{dBi}$. The working frequency of the system is considered to be $868\,\mathrm{MHz}$. A realistic value for the differential RCS is obtained from the research in [59] in which measurements were performed on an NXP UCODE 7 RFID tag. The RCS value is reported to be $-15\,\mathrm{dBsm}$ or $0.0316\,\mathrm{m}^2$ at $868\,\mathrm{MHz}$. For the noise figure, we took the TI™ CC2590 $2.4\,\mathrm{GHz}$ RF front-end as an example, providing a worst-case representative number of around $5\,\mathrm{dB}$ [60, Figure 3].

To obtain baseline target numbers regarding data rates and communication ranges to be achieved, we rely on the use cases drawn up in Deliverable 1.1 [1]. Table 6.2 gives an overview of the use cases where RF backscattering is used by EN devices for uplink communication. It provides both minimum and maximum values on the data rates targeted for the listed applications, along with typical venue scenarios where these may be deployed. Table 6.3 provides realistic area sizes for those venue scenarios.

Table 6.1: Overview of the true-to-life channel and component parameters in the calculation of the required RW resources.

Physical modality	Symbol	Value
Antenna gains	$G_{\mathrm{t}}, G_{\mathrm{r}}$	$2.15\,\mathrm{dBi}$
Wavelength	λ @ $868\,\mathrm{MHz}$	$0.345\,\mathrm{m}$
Differential RCS	$\Delta\sigma$	$-15\,\mathrm{dBsm}$
Noise figure	F	$5\,\mathrm{dB}$

Table 6.2: Typical data rates and venue scenarios for use cases relying on RF backscattering (based on D1.1 [1]).

Application	Minimum data rate [kbps]	Maximum data rate [kbps]	Typical venue
Patient monitoring	0.1	1000	Hospitals, care environments
Tracking of goods	100	1000	Warehouses, sales floor, hospitals
Patient finding	1	1	Hospitals, care environments
People tracking in large venues	1	1000	Factories, events, schools, hospitals
Position tracking of robots and UVs	1000	10000	Factories, hospitals, care environments
Smart home automation	50	50	Home

Based on the established Shannon-Hartley equation (Eq. 6.7) we are able to determine the minimum RW resources needed to cover the distances d_1 and d_2. By RW resources we mean two parameters that can be dynamically and easily adjusted by the RW infrastructure to compensate for a larger total backscatter communication distance, which are the total transmit power P_{t} (within regulatory boundaries) and the array gain G_{array}. Equation (6.9) shows the rearranged Shannon-Hartley equation (Eq. 6.7) with P_{t} and G_{array} isolated. From this formula it is clear that $P_{\mathrm{t}} \cdot G_{\mathrm{array}}$ should be increased proportionally to the square of $(d_1 \cdot d_2)$ in order to achieve the desired range.

$$G_{\mathrm{array}} P_{\mathrm{t}} \geq \frac{(4\pi)^3 (e^{\frac{R_{\max} \ln 2}{B}} - 1) P_{\mathrm{noise}} (d_1 d_2)^2}{\Delta\sigma \lambda^2 G_{\mathrm{t}} G_{\mathrm{r}}} \tag{6.9}$$

Figure 6.2 shows the minimum RW resources $P_{\mathrm{t}} \cdot G_{\mathrm{array}}$ in function of the product $d_1 \cdot d_2$ for typical application data rates as presented in Table 6.2. Two cases are depicted. Figure 6.2a shows the scenario where the fraction of the available bandwidth B to the maximum data rate $R_{\max}$ is 10 $\left[\frac{\mathrm{bps}}{\mathrm{Hz}}\right]$. Figure 6.2b shows the case for a ratio of 5 $\left[\frac{\mathrm{bps}}{\mathrm{Hz}}\right]$.

Table 6.3: Typical area sizes for venue scenarios in Table 6.2 (based on D1.1 [1]).

Venue	Realistic area size
Production hall	$140\,\mathrm{m}$ x $70\,\mathrm{m}$ x $15\,\mathrm{m}$ height
Supermarket	$60\,\mathrm{m}$ x $30\,\mathrm{m}$ x $5\,\mathrm{m}$ height
Large apartment	$15\,\mathrm{m}$ x $10\,\mathrm{m}$ x $2.5\,\mathrm{m}$ height
Hospital floor	$20\,\mathrm{m}$ x $75\,\mathrm{m}$ x $3.5\,\mathrm{m}$ height

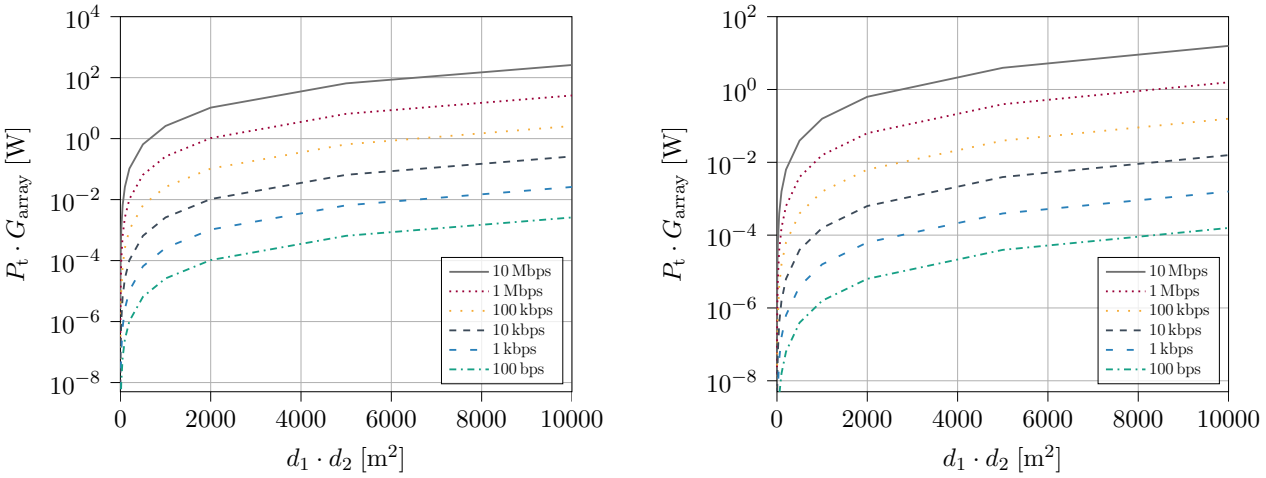

(a) Case $\frac{R_{\max}}{B} = 10 \left[\frac{\text{bps}}{\text{Hz}}\right]$ **(b)** Case $\frac{R_{\max}}{B} = 5 \left[\frac{\text{bps}}{\text{Hz}}\right]$

Figure 6.2: Minimum RW resources $P_t \cdot G_{array}$ needed to cover $d_1 \cdot d_2$ for several targeted data rates. Figure (a) and (b) show the cases where the fraction of the maximum data rate to available bandwidth is respectively 10 and 5 $\left[\frac{\text{bps}}{\text{Hz}}\right]$.

As an example, let us consider the application of position tracking of robots and UVs in a production hall as it poses the most challenges regarding RF backscattering. In this regard, let us assume that the maximum targeted data rate of $10\,000\,\text{kbps}$ is needed, and that the transmitters, receivers, and EN device are maximally distant from each other. In the case of the production hall, this means that $d_1 \cdot d_2$ will be in the range of $10\,000\,\text{m}^2$. If we assume that the selected transmitters in the MISO system contribute more or less equally, the array gain G_{array} will be equal to the number of RW transmitters L. Consequently, $P_t \cdot G_{\text{array}}$ can be rewritten as $P_{t,\text{single}} \cdot L^2$, where $P_{t,\text{single}}$ is the transmit power of a single RW transmitter. Assuming $P_{t,\text{single}} = 20\,\text{dBm}$ for a low power transmitter and that a lower bandwidth is most preferable in general, Figure 6.2a shows that at least $L \approx 51$ transmitters are needed to cover the targeted d_1 and d_2. The number of transmitters can be relaxed by increasing the available bandwidth B, as shown in Figure 6.2b. In this case, a minimum $L \approx 13$ transmitters are needed.

In conclusion, the instantiated Shannon-Hartley equation (Eq. 6.9) and derived graphs in Figure 6.2 allow to calculate the minimum required RW resources to enable RF backscattering over distances d_1 and d_2. They show that $P_t \cdot G_{\text{array}}$ increases linearly with the product of distances d_1 and d_2 squared. Depending on other application parameters such as the targeted data rate and available bandwidth, a different amount of transmitters will have to allocated to guarantee proper decoding at the receiver.

6.3 Separating simultaneously backscattered signals

Energy-neutral devices form a special case when it comes to the multiple access communication problem, with RFID being a prime case hereof. First of all, RFID tags have very limited computing and energy resources available. As a result, they are unable to sense the communication medium themselves and hence are unaware of other transmitting tags in the vicinity. At least they are unable to do so directly, because collision information can be passed on indirectly by the RFID reader who is able to monitor the communication medium and detect collisions. However, this

resource inequality constitutes a first limiting factor in multiple access design for EN devices compared to other communication systems. On the other hand, the amount of power available to an EN device can be very volatile, which can significantly affect its availability and thus response timing.

In a traditional RFID application, often a single reader is considered to read out tags. The RW infrastructure changes this restriction as multiple (dislocated) transmitters and receivers can be allocated to perform this task. This chapter investigates new opportunities in multiple access protocol design.

The following sub-section discusses traditional multiple access solutions that fit the constraints of EN devices. RFID serves as a baseline for this study given its close connection. The section thereafter studies state-of-the-art solutions that can exploit the advantages of the RW infrastructure.

6.3.1 Traditional multiple access solutions for energy-neutral devices

6.3.1.1 Types of collisions

RFID collisions can be split up in tag collisions and reader collisions. The latter can be divided in two other subgroups: reader-tag collisions and reader-reader collisions [61].

Tag collisions occur when multiple tags respond at the same time while being interrogated by an RFID reader. As EN tags typically are unable to detect transmissions of neighboring tags, anti-collision protocols are vital for a good operation performance. This is especially necessary in use cases where a lot of tags are densely packed together, e.g., in stores or productions halls. In a conventional approach after all, the tags are powered by the same reader power field, which makes it likely that they will respond at the same time. The more collisions occur, the more bandwidth and resources are wasted, unless some collision recovery strategy can be used to successfully read the data [62].

Reader-tag collisions occur when the transmit signals from a second reader interfere with tag messages received at another reader. Reader-reader collisions occur when a tag is interrogated by multiple readers at the same time, which might cause the entire reading procedure to fail for both readers.

In many practical RFID systems, tag collisions take more place than reader collisions [61]. However, as the RW infrastructure allows for many readers at the same time, reader interference may have significant more impact on the system performance.

6.3.1.2 Collision-avoiding protocols

Many collision-avoiding protocols have been developed and can be broadly categorized in four main groups: spatial-division multiple access (SDMA), frequency-division multiple access (FDMA), code division-multiple access (CDMA) and time division-multiple access (TDMA) protocols. These protocols belong to group of orthogonal multiple access (OMA) protocols.

SDMA

In space-division multiple access protocols, the space dimension is used to create multiple parallel channels. Directional antennas or phased antenna arrays can for example be used to only

read out tags located in specific spatial areas. One could also divide tags based on their distance to the reader, but this requires many more readers to cover all the tags. Due to intricate antenna design and their increased complexity, these systems have been considered too expensive for many applications in conventional infrastructures. Consequently, their use has been restricted to a few specific applications such as race timing in marathons [63]. Nonetheless, this multiple-access approach could fit naturally in a distributed environment where many low-cost transmitters are used.

FDMA

Frequency-division multiple access protocols separate communication channels using different carrier frequencies. In RFID, the reader uses a fixed frequency for communication in the downlink. If multiple readers are used, a different frequency band can be assigned to each of them. In the uplink, the tags use a variable carrier frequency to transmit signals back to the reader. As in the case of SDMA, a more complex reader design is obtained, which may again be considered too expensive in conventional applications or environments. A distributed infrastructure, on the other hand, serving many applications at the same time may significantly benefit from this multiple-access approach.

CDMA

Code-division multiple access protocols use a special coding scheme and spreading techniques to enable multiple parallel communication channels. A different code is assigned to each tag, often a pseudo-noise (PN) sequence. A tag must multiply this PN code with its message before transmission. The reader must use the same sequence to be able to decode the received signal. While CDMA systems have a higher noise immunity, the channel capacity is not large. Moreover, the design complexity of the tag is higher and the additional computations require more energy [64].

TDMA

Time-division multiple access protocols represent the largest group of anti-collisions protocols in RFID. These protocols divide the entire channel capacity in many time slots. One or multiple time slots can then be allocated for communication with a specific tag.

The protocols can be categorized in either reader-driven or tag-driven [65], also known as reader talks first (RTF) and tag talks first (TTF) respectively. In the former group, the tags remain silent until they are addressed by the reader device, while in the latter tags announce their presence to the reader by transmitting their ID first. Most applications use a RTF procedure, as tag-driven approaches perform relatively slow and tend to be inflexible [64], [65].

6.3.2 Solutions in RW infrastructure

RW brings the advantage of many transceivers that can be allocated on the fly. While SDMA techniques were rather limited to statically directed antenna or phased antenna setups, multiple transmitters and receivers can now be combined to obtain dynamically changing MISO configurations.

mMIMO allows multiplexing between many uncorrelated channels in the space domain effectively creating separate spatial streams. In this way, multiple tags can be read out simultaneously in specifically targeted locations. Once communication with one or multiple tags is complete, the spatially constructed beams can be adapted very quickly to read out tags at other locations. This significantly increases the global capacity of the system. In addition to an increased capacity, one can also use antenna resources to improve the SNR and consequently, lower the bit error rate (BER) and/or extend the reverse-link interrogation range (RIR). The increased throughput and extra reliability can be of particular interest in applications where a large number of tags need to be read or accurate tracking is required [66]. An overview of recent anti-collisions techniques considering MIMO configurations is presented in [66]. More recently, backscattering approaches are also considered in mMIMO networks operating from a central array, including theoretical work in [67] and some first experimental validation in [68]. These studies confirm that mMIMO and large array-based reception can improve the performances of a backscattering system, including multi-tag support.

Referring to the discussion on creating power spots resulting from coherent distributed operation in Section 3.3.1, there is a clear potential for spatial multiplexing multiple simultaneous backscattering devices with a RadioWeaves infrastructure. Contrary to the case where only WPT is intended (as in Section 3.3.1), in collision-avoidance beam isolation is desired rather than beam sharing. This could be attained by establishing dedicated federations and grouping of nodes with similar approaches, as presented by Fitzgerald, Pióro, Tataria, Callebaut, Gunnarsson, and Van der Perre in [69]. The case of backscattering with many devices is indeed similar to how one would address multiple access for purely communication purposes, i.e., group devices based on distinct (orthogonal) channels.

Next to OMA protocols, nonorthogonal multiple access (NOMA) techniques have been presented as candidate for 6G networks [70]. As the number of tags increases, it becomes more challenging to allocate a unique, uncorrelated channel for reader-tag communication. In NOMA, multiple tags could be allowed to share the same frequency band, time or code. Compared to OMA, NOMA is claimed to have the potential to enhance the overall multi-user capabilities, provided the multiple signals can be decoded. Furthermore, NOMA has also been introduced in MIMO to form NOMA-MIMO networks, pushing towards mass connectivity and high spectrum efficiency [70]. While NOMA may open some promising possibilities, it is not our intention to pursue these strategies in REINDEER, where we rather focus on the unprecedented spatial resolution in RadioWeaves.

Chapter 7

Summary and conclusions

This deliverable adress the requirements at the RadioWeaves infrastructure side to support the wireless power transfer functionality, zooming in on the radios in particular. It has taken as a starting point the use cases considered in REINDEER, and further elaborated specifically the electronic shelf label (ESL) case that was identified as most challenging from the wireless power transfer (WPT) perspective. For applications requiring data transfer from the energy neutral (EN) devices, requirements and approaches for backscattering are also handled in a specific chapter.

A major conclusion to be drawn from the different options that are analysed, is that a spectacular efficiency gain can be achieved from coherent multiple-input single-output (MISO) operation with a high number of distributed transmit antennas. Moreover, this can be achieved with relatively low output power power amplifiers (PAs), which is a major asset in view of implementing the WPT features of the contact service points (CSPs) with low cost/low complexity hardware. All use cases considered in combination with the deployment scenarios put forward in this project, can be served with coherent MISO transmission within the applicable regulatory constraints. This does require specific means and procedures to support coherent operation, including synchronization and reciprocity calibration and RF front-ends with phase shifting and detecting capabilities. Yet it is noted that the sensitivity to, e.g., phase errors is not as high as for example for communication purposes.

Furthermore, based on the analysis of hardware requirements, it is advised to provide separate RF front-ends for the WPT functionality, while digital processing and control could be easier shared with resources foreseen for other purposes, e.g., communication. It is also clear from the assessment that the RF front-ends dedicated for WPT can be low-complexity.

Interesting opportunities to increase overall energy efficiency and support a very large number of devices have been identified from beamsharing for WPT specifically on the one hand, and spatial multiplexing based on uncorrelated channels for backscattering devices on the other hand. Establishing dedicated federations of resources to that end can be a way forward to realize this potential.

It should be noticed that in the study reported on in this deliverable, the main focus is on assessing the required (total) transmit power from the infrastructure to the EN nodes, and methods to improve the efficiency on the link. Furthermore, the selection of the PA is discussed, as this can be expected to be a major contributor to inefficiency, and the impact of operating it near to saturation has been clarified. In view of the total energy consumption in the infrastructure, one should consider the bigger picture when establishing federations and thereby taking decisions on

which antennas (not) to use, including potential overhead for example in control and interconnect.

In follow-up, validation of the results reported here is planned in the project. This will include both experimental validation involving real-life transmission in WP5 and simulation-based assessment for diverse use cases in WP1 (Task 1.3). In order to ensure successful validation, some requirements will be further refined, such as the ones relating to the reciprocity calibration.

Appendix A

Synchronization loss

Given the synchronization phase errors φ_ℓ in (4.2), we derive the expected received power as

$$\begin{aligned}\mathbb{E}\left\{P_{\mathrm{rx}}\right\} &= \mathbb{E}\left\{|y|^2\right\} = \mathbb{E}\left\{\left|\boldsymbol{h}^{\mathsf{T}}\boldsymbol{s}+n\right|^2\right\} = \mathbb{E}\left\{\left(\boldsymbol{h}^{\mathsf{T}}\boldsymbol{s}+n\right)^*\left(\boldsymbol{h}^{\mathsf{T}}\boldsymbol{s}+n\right)\right\} \\ &= \mathbb{E}\left\{\left(\boldsymbol{h}^{\mathsf{H}}\boldsymbol{s}^*\right)\left(\boldsymbol{h}^{\mathsf{H}}\boldsymbol{s}^*\right)^*\right\} + \underbrace{2\,\mathbb{E}\left\{\left(\boldsymbol{h}^{\mathsf{H}}\boldsymbol{s}^*\right)n\right\}}_{=0} + \underbrace{\mathbb{E}\left\{n^*\,n\right\}}_{=\sigma_n^2=P_n},\end{aligned} \tag{A.1}$$

where the second term is 0, because

$$\mathbb{E}\left\{\left(\boldsymbol{h}^{\mathsf{H}}\boldsymbol{s}^*\right)n\right\} = \frac{\sqrt{P_{\mathrm{tx}}}}{\|\boldsymbol{h}\|}\underbrace{\mathbb{E}\left\{n\right\}}_{=0}\mathbb{E}\left\{\sum_\ell h_\ell^* h_\ell e^{-j\,\varphi_\ell}\right\} \tag{A.2}$$

due to the statistical independence of n and φ_ℓ.

While the third term in (A.1) corresponds to (unintentional) energy harvesting (EH) of the noise power P_n, the first term corresponds to (intentional) WPT. Its efficiency is given by

$$\begin{aligned}PG_{\mathsf{R}} &= \frac{1}{P_{\mathrm{tx}}}\mathbb{E}\left\{\left(\boldsymbol{h}^{\mathsf{H}}\boldsymbol{s}^*\right)\left(\boldsymbol{h}^{\mathsf{H}}\boldsymbol{s}^*\right)^*\right\} = \frac{1}{\|\boldsymbol{h}\|^2}\mathbb{E}\left\{\left(\sum_\ell |h_\ell|^2 e^{-j\,\varphi_\ell}\right)\left(\sum_\ell |h_\ell|^2 e^{-j\,\varphi_\ell}\right)^*\right\} \\ &= \frac{1}{\|\boldsymbol{h}\|^2}\left(\underbrace{\mathbb{E}\left\{|h_1|^4 e^{j(\varphi_1-\varphi_1)}+\dots\right\}}_{=\sum_\ell |h_\ell|^4=\|\boldsymbol{h}\|_4^4} + \underbrace{\mathbb{E}\left\{|h_1|^2|h_2|^2 e^{j(\varphi_2-\varphi_1)}+|h_1|^2|h_3|^2 e^{j(\varphi_3-\varphi_1)}+\dots\right\}}_{=2\binom{L}{2}G_{\mathrm{ch}}^2\mathbb{E}\left\{e^{j2\varphi_\ell}\right\}}\right) \\ &= \frac{\mathbb{E}\left\{\left|\boldsymbol{h}^{\mathsf{T}}\boldsymbol{s}\right|^2\right\}}{P_{\mathrm{tx}}} = \frac{1}{\|\boldsymbol{h}\|^2}\left(\|\boldsymbol{h}\|_4^4 + 2\binom{L}{2}G_{\mathrm{ch}}^2 e^{-\sigma_\varphi^2}\right),\end{aligned} \tag{A.3}$$

since the phase errors φ_ℓ are assumed i.i.d. zero-mean Gaussian and it can be shown that $\mathbb{E}\left\{e^{j2\varphi_\ell}\right\} = e^{-\sigma_\varphi^2} \triangleq G_{\mathsf{SYNC}}$.

Bibliography

[1] J. F. Esteban and M. Truskaller, "Use case-driven specifications and technical requirements and initial channel model," REINDEER project, Deliverable ICT-52-2020 / D1.1, Sep. 2021. DOI: 10.5281/zenodo.5561844.

[2] O. Edfors, "Initial assessment of architectures and hardware resources for a RadioWeaves infrastructure," REINDEER project, Deliverable ICT-52-2020 / D2.1, Jan. 2022. DOI: 10.5281/zenodo.5938909.

[3] R. project, "System design study for energy-neutral devices interacting with the RadioWeaves infrastructure," Deliverable ICT-52-2020 / D4.1, 2022, unpublished.

[4] J. F. Esteban, M. Truskaller, L. Fabrete, A. Stanek, D. Delabie, L. Van der Perre, E. G. Larsson, S. Rimalapudi, E. Fitzgerald, F. Tufvesson, *et al.*, "Use case-driven specifications and technical requirements and initial channel model," 2021.

[5] C. Song, Y. Huang, J. Zhou, P. Carter, S. Yuan, Q. Xu, and Z. Fei, "Matching network elimination in broadband rectennas for high-efficiency wireless power transfer and energy harvesting," *IEEE Transactions on Industrial Electronics*, vol. 64, no. 5, pp. 3950–3961, 2016.

[6] *Highly efficient, regulated dual-output, ambient energy manager for AC or DC sources with optional primary battery*, AEM30940, Rev. 1.4, E-peas, Jun. 2022.

[7] NXP Semiconductors, "SL3S1205 UCODE 8/8m," NXP Semiconductors, product data sheet rev. 3.6, 2021, p. 38. [Online]. Available: https://www.nxp.com/docs/en/data-sheet/SL3S1205_15.pdf.

[8] *Highly-efficient, regulated dual-output, ambient energy manager for high-frequency RF input with optional primary battery*, AEM40940, Rev. 1.1, e-Peas semiconductors, Jan. 2018.

[9] Passive Components Blog. "Leakage Current Characteristics of Capacitors." Visited on 2023-02-20. (2023), [Online]. Available: https://passive-components.eu/leakage-current-characteristics-of-capacitors (visited on 2023).

[10] MathWorks. "Create inset-fed microstrip patch antenna." Visited on 2023-02-20. (2023), [Online]. Available: https://nl.mathworks.com/help/antenna/ref/patchmicrostripinsetfed.html (visited on 2023).

[11] REINDEER Project, "Propagation characteristics and channel models for RadioWeaves including reflectarrays," Deliverable ICT-52-2020 / D1.2, 2023 (unpublished).

[12] S. Claessens, "Simultaneous Wireless Information and Power Transfer without Local Oscillator," 2020.

[13] D. Pavone, A. Buonanno, M. D'Urso, and F. G. D. Corte, "DESIGN CONSIDERATIONS FOR RADIO FREQUENCY ENERGY HARVESTING DEVICES," *Progress in Electromagnetics Research B*, vol. 45, pp. 19–35, 2012.

[14] Z. Li, M. Zeng, and H.-Z. Tan, "A multi-band rectifier with modified hybrid junction for RF energy harvesting," *Microwave and Optical Technology Letters*, vol. 60, pp. 817–821, Apr. 2018. DOI: 10.1002/mop.31057.

[15] S. Roy, J.-J. Tiang, M. B. Roslee, M. T. Ahmed, A. Z. Kouzani, and M. A. P. Mahmud, "Design of a Highly Efficient Wideband Multi-Frequency Ambient RF Energy Harvester," *Sensors*, vol. 22, no. 2, 2022, ISSN: 1424-8220. DOI: 10.3390/s22020424. [Online]. Available: https://www.mdpi.com/1424-8220/22/2/424.

[16] S. Keyrouz, H. J. Visser, and A. G. Tijhuis, "Multi-band simultaneous radio frequency energy harvesting," in *2013 7th European Conference on Antennas and Propagation (EuCAP)*, 2013, pp. 3058–3061.

[17] Y.-H. Suh and K. Chang, "A high-efficiency dual-frequency rectenna for 2.45- and 5.8-GHz wireless power transmission," *IEEE Transactions on Microwave Theory and Techniques*, vol. 50, no. 7, pp. 1784–1789, 2002. DOI: 10.1109/TMTT.2002.800430.

[18] C. Buyle, B. Cox, L. Van der Perre, and L. De Strycker, *A Multi-band Solution for Interacting with Energy-Neutral Devices*, 2022.

[19] N. Shariati, J. R. Scott, D. Schreurs, and K. Ghorbani, "Multitone excitation analysis in RF energy harvesters - Considerations and limitations," *IEEE Internet of Things Journal*, vol. 5, no. 4, pp. 2804–2816, 2018.

[20] R. project, "Signal processing for WPT and uplink signalling, exploiting environment awareness," Deliverable ICT-52-2020 / D4.2, 2023, unpublished.

[21] F. Bolos, J. Blanco, A. Collado, and A. Georgiadis, "RF energy harvesting from multi-tone and digitally modulated signals," *IEEE Transactions on Microwave Theory and Techniques*, vol. 64, no. 6, pp. 1918–1927, 2016.

[22] B. Clerckx and E. Bayguzina, "Low-complexity adaptive multisine waveform design for wireless power transfer," *IEEE Antennas and Wireless Propagation Letters*, vol. 16, pp. 2207–2210, 2017.

[23] Y. Huang and B. Clerckx, "Large-scale multiantenna multisine wireless power transfer," *IEEE Transactions on Signal Processing*, vol. 65, no. 21, pp. 5812–5827, 2017. DOI: 10.1109/TSP.2017.2739112.

[24] Y. Zhang and B. Clerckx, "Waveform optimization for wireless power transfer with power amplifier and energy harvester non-linearities," in *ICASSP 2022 - 2022 IEEE International Conference on Acoustics, Speech and Signal Processing (ICASSP)*, 2022, pp. 8632–8636. DOI: 10.1109/ICASSP43922.2022.9746380.

[25] G. EPCglobal, "EPC Radio-Frequency Identity Protocols Generation-2 UHF RFID - Specification for RFID Air Interface - Protocol for Communications at 860 mhz–960 mhz," *EPCglobal Inc., Apr*, vol. 1, no. Version 2.0.1, p. 152, 2015.

[26] R. project, "Evaluation of the distribution of processing across infrastructure and associated requirements on back-haul and synchronization," Deliverable ICT-52-2020 / D2.2, 2023, unpublished.

[27] B. J. B. Deutschmann, T. Wilding, M. Graber, and K. Witrisal, "XL-MIMO channel modeling and prediction for wireless power transfer," in *WS10 IEEE ICC 2023 Workshop on Near-Field Localization and Communication for 6G (WS10 ICC'23 Workshop - NrFldfCom6G)*, Rome, Italy, May 2023.

[28] Joint Committee for Guides in Metrology, "Guide to the Expression of Uncertainty in Measurement (GUM): Evaluation of Measurement Data," 2008.

[29] A. Bourdoux, B. Come, and N. Khaled, "Non-reciprocal transceivers in OFDM/SDMA systems: impact and mitigation," in *Radio and Wireless Conference, 2003. RAWCON '03. Proceedings*, 2003, pp. 183–186. DOI: 10.1109/RAWCON.2003.1227923.

[30] M. project, "Analysis of non-reciprocity impact and possible solutions," Deliverable ICT-619086 / D2.4, 2015, unpublished.

[31] J. Vieira, F. Rusek, O. Edfors, S. Malkowsky, L. Liu, and F. Tufvesson, "Reciprocity Calibration for Massive MIMO: Proposal, Modeling, and Validation," *IEEE Transactions on Wireless Communications*, vol. 16, no. 5, pp. 3042–3056, 2017. DOI: 10.1109/TWC.2017.2674659.

[32] C.-M. Chen, S. Blandino, A. Gaber, C. Desset, A. Bourdoux, L. Van der Perre, and S. Pollin, "Distributed Massive MIMO: A Diversity Combining Method for TDD Reciprocity Calibration," in *GLOBECOM 2017 - 2017 IEEE Global Communications Conference*, 2017, pp. 1–7. DOI: 10.1109/GLOCOM.2017.8254817.

[33] J. Vieira and E. G. Larsson, "Reciprocity calibration of Distributed Massive MIMO Access Points for Coherent Operation," in *2021 IEEE 32nd Annual International Symposium on Personal, Indoor and Mobile Radio Communications (PIMRC)*, 2021, pp. 783–787. DOI: 10.1109/PIMRC50174.2021.9569495.

[34] R. project, "Position Estimation and Environment Learning," Deliverable ICT-52-2020 / D3.2, 2023, unpublished.

[35] I. C. on Non-Ionizing Radiation Protection *et al.*, "Guidelines for limiting exposure to electromagnetic fields (100 kHz to 300 GHz)," *Health physics*, vol. 118, no. 5, pp. 483–524, 2020.

[36] Jingon Joung. "Energy Efficient Wireless Communications." Visited on 2023-03-08. (2015), [Online]. Available: https://www.slideshare.net/JingonJoung/tutorial-iceic2015 (visited on 2015).

[37] S. C. Cripps *et al.*, *RF power amplifiers for wireless communications*. Artech house Norwood, MA, 2006, vol. 250.

[38] Mini-Circuits. "Monolithic Amplifier PGA-102+." Visited on 2023-03-08. (), [Online]. Available: https://www.minicircuits.com/pdfs/PGA-102+.pdf.

[39] A. Grebennikov, "High-Efficiency Class-E Power Amplifier With Shunt Capacitance and Shunt Filter," *IEEE Transactions on Circuits and Systems I: Regular Papers*, vol. 63, no. 1, pp. 12–22, 2016. DOI: 10.1109/TCSI.2015.2512698.

[40] F. Moloudi and H. Jahanirad, "Broadband class-E power amplifier design using tunable output matching network," *AEU-International Journal of Electronics and Communications*, vol. 118, p. 153 142, 2020.

[41] Energous. "EN3210 - High efficiency wireless power amplifier." Visited on 2023-03-08. (), [Online]. Available: https://energous.com/products/chips-modules/en3210/.

[42] C. Barrett, "Fractional/integer-N PLL basics," 1999.

[43] A. Harney, "Achieving Phase Coherence Between Multiple Fractional-N PLLs ADF4350 Phase Resync and Phase Programmability," *Application Note, Norwood, MA, USA: Analog Devices*, 2010.

[44] *Phase Synchronization of Multiple PLL Synthesizers Reference Design*, V1, Texas Instruments, May 2017.

[45] P. M. Lavrador, T. R. Cunha, P. M. Cabral, and J. Pedro, "The Linearity-Efficiency Compromise," *IEEE Microwave Magazine*, vol. 11, no. 5, pp. 44–58, 2010. DOI: 10.1109/MMM.2010.937100.

[46] E. G. Larsson and L. Van Der Perre, "Out-of-Band Radiation From Antenna Arrays Clarified," *IEEE Wireless Communications Lett.*, vol. 7, no. 4, pp. 610–613, 2018. DOI: 10.1109/LWC.2018.2802519.

[47] C. Mollén, E. G. Larsson, and T. Eriksson, "Waveforms for the Massive MIMO Downlink: Amplifier Efficiency, Distortion, and Performance," *IEEE Trans. on Commun.*, vol. 64, no. 12, pp. 5050–5063, 2016. DOI: 10.1109/TCOMM.2016.2557781.

[48] F. Rottenberg, G. Callebaut, and L. V. der Perre, *Spatial Distribution of Distortion due to Nonlinear Power Amplification in Distributed Massive MIMO*, 2021. arXiv: 2106.10140 [eess.SP].

[49] C. Mollén, U. Gustavsson, T. Eriksson, and E. G. Larsson, "Spatial Characteristics of Distortion Radiated From Antenna Arrays With Transceiver Nonlinearities," *IEEE Trans. on Wireless Commun.*, vol. 17, no. 10, pp. 6663–6679, 2018. DOI: 10.1109/TWC.2018.2861872.

[50] C. Fager, T. Eriksson, F. Barradas, K. Hausmair, T. Cunha, and J. C. Pedro, "Linearity and Efficiency in 5G Transmitters: New Techniques for Analyzing Efficiency, Linearity, and Linearization in a 5G Active Antenna Transmitter Context," *IEEE Microwave Magazine*, vol. 20, no. 5, pp. 35–49, 2019. DOI: 10.1109/MMM.2019.2898020.

[51] F. Rottenberg, G. Callebaut, and L. V. der Perre, *Z3RO Precoder Canceling Nonlinear Power Amplifier Distortion in Large Array Systems*, 2021. arXiv: 2110.07891 [eess.SP].

[52] S. K. Mohammed and E. G. Larsson, "Per-Antenna Constant Envelope Precoding for Large Multi-User MIMO Systems," *IEEE Transactions on Communications*, vol. 61, no. 3, pp. 1059–1071, 2013. DOI: 10.1109/TCOMM.2013.012913.110827.

[53] C. A. Balanis, *Antenna Theory: Analysis and Design*. John Wiley & Sons, 2005, vol. 3, ISBN: 9780471667827.

[54] E. F. Knott, J. F. Schaeffer, and T. M. Tulley, *Radar Cross Section*. USA: SciTech Publishing, 2004, ISBN: 1891121251.

[55] R. B. Green, "The general theory of antenna scattering," Ph.D. dissertation, The Ohio State University, 1963.

[56] P. Nikitin, K. Rao, and R. Martinez, "Differential RCS of RFID tag," *Electronics Letters*, vol. 43, pp. 431–432, Feb. 2007. DOI: 10.1049/el:20070253.

[57] J. F. Ensworth and M. S. Reynolds, "Every smart phone is a backscatter reader: Modulated backscatter compatibility with Bluetooth 4.0 Low Energy (BLE) devices," in *IEEE International Conference on RFID*, 2015, pp. 78–85. DOI: 10.1109/RFID.2015.7113076.

[58] V. Iyer, V. Talla, B. Kellogg, S. Gollakota, and J. Smith, "Inter-Technology Backscatter: Towards Internet Connectivity for Implanted Devices," in *Proceedings of the 2016 ACM SIGCOMM Conference*, Florianopolis, Brazil, 2016, pp. 356–369, ISBN: 9781450341936.

[59] D. Neunteufel, F. Galler, and H. Arthaber, "Comprehensive Measurement of Complex-valued Delta Radar Cross-section," in *2018 6th International EURASIP Workshop on RFID Technology (EURFID)*, 2018, pp. 1–7.

[60] Texas Instruments, "CC2590 2.4-GHz RF Front End, 14-dBm output power," Texas Instruments, product data sheet SWRS080, Sep. 2008, p. 11. [Online]. Available: https://www.ti.com/product/CC2590#tech-docs.

[61] Z. Tang and Y. He, "Research of Multi-access and Anti-collision Protocols in RFID Systems," in *2007 International Workshop on Anti-Counterfeiting, Security and Identification (ASID)*, 2007, pp. 377–380. DOI: 10.1109/IWASID.2007.373659.

[62] C. Angerer, R. Langwieser, and M. Rupp, "RFID Reader Receivers for Physical Layer Collision Recovery," *IEEE Transactions on Communications*, vol. 58, no. 12, pp. 3526–3537, 2010. DOI: 10.1109/TCOMM.2010.101910.100004.

[63] X. Yu, Z. Zhao, X. Zhang, X. Yu, Z. Zhao, and X. Zhang, "Physical theory of RFID system physical anti-collision," *Physical Anti-Collision in RFID Systems: Theory and Practice*, pp. 59–108, 2021.

[64] Z. Tang and Y. He, "Research of multi-access and anti-collision protocols in RFID systems," in *2007 international workshop on anti-counterfeiting, security and identification (ASID)*, IEEE, 2007, pp. 377–380.

[65] D. K. Klair, K.-W. Chin, and R. Raad, "A survey and tutorial of RFID anti-collision protocols," *IEEE Communications surveys & tutorials*, vol. 12, no. 3, pp. 400–421, 2010.

[66] M. Alotaibi, M. Murad, S. A. Alhuthali, F. R. Al-Osaimi, and F. Aldosari, "MIMO Radio Frequency Identification: A Brief Survey," *Sensors*, vol. 22, no. 11, p. 4115, 2022.

[67] A. Al-Nahari, R. Jäntti, D. Mishra, and J. Hämäläinen, "Massive mimo beamforming in monostatic backscatter multi-tag networks," *IEEE Communications Letters*, vol. 25, no. 4, pp. 1323–1327, 2021. DOI: 10.1109/LCOMM.2020.3046690.

[68] R. Fara, N. Bel-Haj-Maati, D.-T. Phan-Huy, N. Malhouroux, and M. Di Renzo, "First experimental evaluation of ambient backscatter communications with massive mimo reader," in *2020 IEEE 31st Annual International Symposium on Personal, Indoor and Mobile Radio Communications*, 2020, pp. 1–6. DOI: 10.1109/PIMRC48278.2020.9217189.

[69] E. Fitzgerald, M. Pióro, H. Tataria, G. Callebaut, S. Gunnarsson, and L. Van der Perre, "A Light Signaling Approach to Node Grouping for Massive MIMO IoT Networks," *Computers*, vol. 11, no. 6, 2022, ISSN: 2073-431X. DOI: 10.3390/computers11060098. [Online]. Available: https://www.mdpi.com/2073-431X/11/6/98.

[70] S. S. Yılmaz, B. Özbek, M. İlgüy, B. Okyere, L. Musavian, and J. Gonzalez, "User Selection for NOMA-Based MIMO With Physical-Layer Network Coding in Internet of Things Applications," *IEEE Internet of Things Journal*, vol. 9, no. 16, pp. 14 998–15 006, 2021.